Supplementary Information

Dual-Emitting Cyclometalated Ir(III) Complexes with Salicylaldimine-Bound Fluorophores for Ratiometric Oxygen Sensing

Sirawit Tidma, Gregory D. Sutton, Linh T. M. Dang, Chenggang Jiang, and Thomas S. Teets

Department of Chemistry, University of Houston, 3585 Cullen Blvd. Room 112, Houston, Tx USA, 77204-5003. E-mail: ttets@uh.edu

Experimental Section

Materials. All chemicals were purchased from commercially available sources and were used without further purification unless otherwise specified. Solvents were deoxygenated and dried using a Grubbs Solvent Purification System. Chloro-bridged cyclometalated iridium dimer precursors, $[Ir(C\hat{}N)_2(\mu\text{-}Cl)_2]$, were prepared by way of Nonoyama,[1] and fluorophores **C3H** and **C4H** were prepared by known methods.[2,3]

Physical methods. ^1H and $^{13}C\{^1H\}$ NMR spectra were recorded at room temperature on a JEOL ECA-400, ECA-500 or ECA-600 NMR spectrometer. UV–vis absorption spectra were recorded in screw-capped 1 cm quartz cuvettes using an Agilent Carey 8454 UV–vis spectrophotometer. Photoluminescence (PL) spectra were obtained at room temperature using a Horiba FluoroMax-4 spectrofluorometer, with samples housed in 1 cm quartz cuvettes with septum-sealed screw caps. Solutions for these measurements were prepared inside a nitrogen-filled glovebox using dry and deoxygenated solvents to exclude air. Luminescence lifetimes were measured with a Horiba DeltaFlex Lifetime System, using pulsed diode excitation at 330 nm. PL wavelengths for lifetime measurements were selected by using appropriate long-pass filters, and the decay trace was fitted using the instrument's analysis software or the software Origin 2020b. PL quantum yields for all complexes were measured relative to a standard tetraphenylporphyrin, which has a reported fluorescence quantum yield (Φ_{Flu}) of 0.11[4]. The quantum yields of the Ir-fluorophore conjugates (Φ_x) were calculated using Equation S1 below, where Φ_{st} = the quantum yield of the standard, m_x = the slope of emission intensity versus absorbance for the samples, m_{st} = the slope of emission intensity versus absorbance for the standard compound, and η_x and η_{st} are the refractive indexes of the solvents of the sample and standard, respectively.

$$\Phi_x = \Phi_{st}\left[\frac{m_x}{m_{st}}\right]\left[\frac{\eta_x}{\eta_{st}}\right]^2 \qquad \text{(S1)}$$

Oxygen quenching experiments. The iridium-coumarin complexes were dissolved in dichloromethane in a nitrogen-filled glovebox. The stock solutions were further diluted into quartz cuvettes to reach a concentration of 1.0×10^{-5} M in each sample. The volume of solution present in each cuvette was 3.0 mL, leaving 0.5 mL of headspace for addition of varying aliquots of air. The PL spectrum for each complex was recorded under nitrogen atmosphere (pO_2 = 0 mmHg), then aliquots of air were added to each cuvette via syringe (100 μL per addition) and the PL spectra were recorded after each aliquot using an excitation wavelength of 310 nm. The process was repeated five total times, reaching an oxygen pressure pO_2 = 160 mmHg, equivalent to the atmospheric oxygen level. The ratio of phosphorescence to fluorescence intensity was plotted versus oxygen partial pressure to obtain Stern-Volmer quenching constants (K_{SV}) for these complexes (Fig. S30–S37). The Stern-Volmer quenching constant K_{SV} and the quenching rate constant (k_q) were calculated for each complex.

X-ray crystal details. Single crystals were grown by vapor diffusion of pentane into nearly saturated dichloromethane solutions. Crystals were mounted on a Bruker Apex II three-circle diffractometer using MoKα radiation (λ = 0.71073 Å). The data was collected at 123(2) K and was processed and refined within the APEXII software. Structures were solved by intrinsic phasing in SHELXT and refined by standard difference Fourier techniques in program SHELXL.[5] Hydrogen atoms were placed in calculated positions using standard riding model and refined isotropically; all non-hydrogen atoms were refined anisotropically. Crystallographic details are summarized in Table S1.

Photodegradation experiments. Iridium-coumarin complexes **piq-C3** and **piq-C**[6] were each dissolved in dichloromethane under aerated conditions. Stock solutions of each complex were further diluted in quartz cuvettes (1 cm path length) to an absorbance of 0.50 at 310 nm. The photodegradation tests were performed by irradiation using a glass bowl wrapped with UV LED strips (λ = 285 nm), and covered on the outside with aluminum foil. To maintain a constant irradiation temperature, the vessel was cooled with a fan. For all experiments, PL spectra were recorded in regular intervals by exciting at 310 nm and recording the spectrum from 350–720 nm.

Syntheses

Synthesis of Coumarin C3H. This compound was prepared by a modified literature procedure.[2] A mixture of 7-amino-4-methyl coumarin (200 mg, 1.14 mmol) and salicylaldehyde (120 µL, 1.15 mmol) in methanol (10 mL) was combined, and then a drop of trifluoroacetic acid was added (formic acid was used in the literature procedure). The reaction was refluxed overnight, then filtered, and the product was washed with cold methanol and pentane to give an orange solid. Yield: 185 mg (58%). ^{1}H NMR (400 MHz, $CDCl_3$): δ = 8.64 (s, 1H, N=C*H*), 7.64 (d, 1H, *J* = 8.2 Hz, Ar*H*), 7.42 (t, 2H, *J* = 7.9 Hz, Ar*H*), 7.19–7.23 (m, 2H, Ar*H*), 7.04 (d, 1H, *J* = 8.1 Hz, Ar*H*), 6.97 (t, 1H, *J* = 7.5 Hz, Ar*H*), 6.27 (s, 1H, lactone C=C*H*), 2.45 (s, 3H, CH_3).

Synthesis of Coumarin C4H. This compound was prepared as described in the literature.[3] (1) A solution of 7-amino-4-methyl coumarin (175 mg, 1.00 mmol) in 5 mL of concentrated HCl was prepared. Sodium nitrite (80 mg, 1.2 mmol) in deionized water (3 mL) was then added dropwise. The reaction was stirred for an hour at a maintained temperature between −5 °C to 0 °C. After that the mixture was poured into a prepared cold solution of stannous chloride dihydrate (0.72 g, 3.2 mmol) in 7.2 mL of concentrated HCl. Stirring was continued for an hour at a maintained temperature below 0 °C, then the solid was filtered and washed with cold water, alcohol, and diethyl ether respectively to get the light-yellow solid of coumarin hydrazine: Yield 183 mg (96%) ^{1}H NMR (400 MHz, DMSO-d_6): δ = 9.40 (br, 2H, NH_2), 8.66 (s, 1H, N=C*H*), 7.60 (d, 1H, *J* = 8.7 Hz, Ar*H*), 6.83 (dd, 1H, *J* = 8.8, 1.8 Hz, Ar*H*), 6.77 (d, 1H, *J* = 2.1 Hz, Ar*H*), 6.10 (s, 1H, lactone C=C*H*), 2.33 (s, 3H, CH_3).

(2) A solution of salicylaldehyde (0.60 mL, 5.8 mmol) in methanol (3 mL) was poured into a prepared mixture solution of coumarin hydrazine (0.11 g, 0.58 mmol) in methanol (5 mL) with a few drops of trifluoroacetic acid. Stirring was continued for 30 min, then the product was filtered and washed with cold alcohol and diethyl ether to get a yellow solid of coumarin **C4H**: (Yield 78 mg, 47%) ^{1}H NMR (500 MHz, DMSO-d_6): δ = 10.94 (s, 1H, O*H*), 10.16 (s, 1H, N*H*), 8.23 (s, 1H, N=C*H*), 7.67 (dd, 1H, *J* = 7.7, 1.7 Hz, Ar*H*), 7.58 (d, 1H, *J* = 8.7 Hz, Ar*H*), 7.14–7.18 (m, 1H, Ar*H*), 6.91 (dd, 1H, *J* = 8.7, 2.1 Hz, Ar*H*), 6.82–6.86 (m, 3H, Ar*H*), 6.03 (d, 1H, *J* = 1.1 Hz, C=C*H*), 2.32 (s, 3H, CH_3).

General procedure for the preparation of cyclometalated iridium-coumarin complexes. 1 equivalent of the chloro-bridged cyclometalated iridium dimer $[Ir(C^N)_2(\mu\text{-}Cl)]_2$ was treated with 20 equivalents of Na_2CO_3 or TEA (triethylamine) in 10 mL of reagent alcohol and stirred for 1 h, and then 2 equivalents of the respective coumarin ligand (**C3H** or **C4H**) were added. The reaction mixture was refluxed for 3–5 days. The solvent was removed under vacuum, and then the residue was redissolved in CH_2Cl_2 followed by filtration through a thin layer of alumina using CH_2Cl_2 as the eluent to flush the product out. After removing the solvent under vacuum, the remaining solid was further purified by precipitation from CH_2Cl_2/C_5H_{12} (1:5 v/v) to obtain a solid.

Synthesis of piq-C3. This complex was prepared according to general procedure using $[Ir(piq)_2(\mu\text{-}Cl)]_2$ (54 mg, 0.041 mmol), an excess of Na_2CO_3 (85 mg, 0.80 mmol), and **C3H** (22 mg, 0.079 mmol). The reaction was refluxed for 3 days. The product was obtained as a red solid. Yield: 23 mg (33%). ^{1}H NMR (400 MHz, $CDCl_3$): δ = 8.95 (d, 1H, *J* = 9.6 Hz, Ar*H*), 8.84 (d, 1H, *J* = 6.4 Hz, Ar*H*), 8.74 (d, 1H, *J* = 6.4 Hz, Ar*H*), 8.44 (d, 1H, *J* = 8.5 Hz, Ar*H*), 8.17 (d, 1H, *J* = 8.5 Hz, Ar*H*), 8.10 (s, 1H, N=C*H*), 7.94 (d, 1H, *J* = 8.3 Hz, Ar*H*), 7.88–7.90 (m, 1H, Ar*H*), 7.68–7.73 (m, 3H, Ar*H*), 7.58 (t, 1H, *J* = 8.6 Hz, Ar*H*), 7.54 (d, 1H, *J* = 8.3 Hz, Ar*H*), 7.49 (d, 1H, *J* = 6.4 Hz, Ar*H*), 7.39 (d, 1H, *J* = 6.3 Hz, Ar*H*), 7.20 (t, 1H, *J* = 6.8 Hz, Ar*H*), 7.12 (d, 1H, *J* = 7.2 Hz, Ar*H*), 6.92 (t, 1H, *J* = 7.6 Hz, Ar*H*), 6.76 (d, 1H, *J* = 8.6 Hz, Ar*H*), 6.63–6.69 (m, 2H, Ar*H*), 6.48 (dt, 2H, *J* = 19.8, 7.0 Hz, Ar*H*), 6.39 (t, 1H, *J* = 7.3 Hz, Ar*H*), 6.32 (d, 1H, *J* = 7.6 Hz, Ar*H*), 6.22 (d, 1H, *J* = 7.5 Hz, Ar*H*), 6.20 (d, 1H, *J* = 10 Hz, Ar*H*), 6.07 (s, 1H, lactone C=C*H*), 6.02 (d, 2H, *J* = 8.6 Hz, Ar*H*), 2.21 (s, 3H, CH_3). ^{13}C{^{1}H} NMR (151 MHz, $CDCl_3$): δ = 169.8, 169.1, 167.6, 161.3, 160.7, 154.5, 154.3, 154.2, 152.7, 151.9, 146.3, 145.6, 141.6, 140.7, 137.1, 136.9, 135.4, 134.8, 133.9, 133.1, 130.9, 130.9, 129.9, 129.4, 129.3, 129.2, 127.9, 127.7, 127.6, 127.2, 126.6, 126.3, 126.0, 125.3, 123.4, 121.4, 121.2, 120.2, 120.1, 119.4, 119.2, 116.7, 113.9, 113.8, 111.3, 18.7.

Synthesis of pphen-C3. This complex was prepared in the glove box using $[Ir(pphen)_2(\mu\text{-}Cl)]_2$ (54 mg, 0.038 mmol), an excess of TEA (0.1 mL, 0.8 mmol), and **C3H** (22 mg, 0.079 mmol) in 5 mL of CH_2Cl_2. The reaction was stirred at room temperature under N_2 gas for 5 days. The crude product was filtered through a thin layer of alumina, using CH_2Cl_2 as an eluent to flush the product out, and then further purified

by precipitation from CH_2Cl_2/C_5H_{12} (1:5 v/v) to give a brown solid. Yield: 32 mg (43%). ^{1}H NMR (600 MHz, $CDCl_3$): δ = 9.38 (d, 1H, *J* = 8.5 Hz, Ar*H*), 9.17 (d, 1H, *J* = 8.2 Hz, Ar*H*), 8.61 (d, 1H, *J* = 8.6 Hz, Ar*H*), 8.53 (d, 1H, *J* = 8.4 Hz, Ar*H*), 8.44 (d, 1H, *J* = 8.3 Hz, Ar*H*), 8.41 (d, 1H, *J* = 7.9 Hz, Ar*H*), 8.31 (d, 1H, *J* = 8.2 Hz, Ar*H*), 8.19 (dd, 2H, *J* = 8.6, 4.1 Hz, Ar*H*), 7.88 (d, 1H, *J* = 7.9 Hz, Ar*H*), 7.85 (t, 1H, *J* = 7.7 Hz, Ar*H*), 7.78 (t, 1H, *J* = 7.7 Hz, Ar*H*), 7.67 (t, 1H, *J* = 7.7 Hz, Ar*H*), 7.50–7.55 (m, 2H, Ar*H*), 7.45 (t, 1H, *J* = 7.5 Hz, Ar*H*), 7.37 (t, 1H, *J* = 7.5 Hz, Ar*H*), 7.33 (t, 1H, *J* = 7.7 Hz, Ar*H*), 7.17 (s, 1H, N=C*H*), 7.07 (d, 1H, *J* = 7.7 Hz, Ar*H*), 7.00 (t, 1H, *J* = 7.5 Hz, Ar*H*), 6.69 (t, 1H, *J* = 7.5 Hz, Ar*H*), 6.70 (d, 1H, *J* = 8.2 Hz, Ar*H*), 6.67 (t, 1H, *J* = 7.4 Hz, Ar*H*), 6.60 (t, 1H, *J* = 7.4 Hz, Ar*H*), 6.52 (d, 1H, *J* = 7.7 Hz, Ar*H*), 6.30 (t, 1H, *J* = 7.5 Hz, Ar*H*), 6.16 (d, 1H, *J* = 7.6 Hz, Ar*H*), 6.11 (s, 1H, lactone C=C*H*), 6.05–6.07 (m, 2H, Ar*H*), 5.74–5.77 (m, 2H, Ar*H*), 2.14 (s, 3H, CH_3). ^{13}C{^{1}H} NMR (151 MHz, $CDCl_3$): δ = 174.2, 174.0, 170.1, 165.2, 160.6, 153.2, 152.9, 152.8, 152.2, 151.8, 148.6, 147.5, 145.1, 143.7, 137.6, 135.2, 134.0, 133.9, 133.7, 133.3, 132.0, 131.5, 131.1, 131.0, 130.5, 129.5, 129.2, 129.0, 128.2, 127.7, 127.2, 127.0, 126.8, 126.0, 125.8, 125.5, 124.1, 123.9, 123.7, 123.4, 122.52, 122.49, 122.4, 122.01, 121.99, 121.6, 121.5, 119.8, 118.9, 117.5, 114.0, 113.0,110.6, 18.6. One ^{13}C resonance was not clearly located.

Synthesis of bt-C3. This complex was prepared according to general experimental preparation using $[Ir(bt)_2(\mu\text{-}Cl)]_2$ (52 mg, 0.040 mmol), an excess of TEA (0.1 mL, 0.8 mmol) and **C3H** (22 mg, 0.079 mmol). The reaction was refluxed for 4 days. The product was obtained as an orange solid. Yield: 34 mg (45%). ^{1}H NMR (600 MHz, $CDCl_3$): δ = 8.59 (d, 1H, *J* = 8.2 Hz, Ar*H*), 8.19 (d, 1H, *J* = 8.0 Hz, Ar*H*), 7.98 (s, 1H, N=C*H*), 7.84–7.87 (m, 2H, Ar*H*), 7.66 (d, 1H, *J* = 7.6 Hz, Ar*H*), 7.41 (t, 1H, *J* = 7.5 Hz, Ar*H*), 7.35–7.39 (m, 3H, Ar*H*), 7.16 (t, 1H, *J* = 6.7 Hz, Ar*H*), 7.01 (d, 1H, *J* = 8.3 Hz, Ar*H*), 6.96 (d, 1H, *J* = 8.3 Hz, Ar*H*), 6.65–6.89 (m, 2H, Ar*H*), 6.69 (d, 1H, *J* = 8.7 Hz, Ar*H*), 6.66 (t, 1H, *J* = 7.3 Hz, Ar*H*), 6.55 (t, 1H, *J* = 6.6 Hz, Ar*H*), 6.52 (t, 1H, *J* = 7.3 Hz, Ar*H*), 6.34 (d, 2H, *J* = 7.6 Hz, Ar*H*), 6.28 (t, 1H, *J* = 7.3 Hz, Ar*H*), 6.17–6.19 (m, 2H, Ar*H*), 6.13 (s, 1H, lactone C=C*H*), 2.28 (s, 3H, CH_3). ^{13}C{^{1}H} NMR (151 MHz, $CDCl_3$): δ = 181.4, 180.5, 168.6, 163.2, 160.9, 154.4, 152.8, 152.0, 151.5, 151.3, 150.9, 150.7, 141.5, 141.1, 135.3, 134.9, 134.8, 133.7, 131.4, 131.1, 130.8, 128.3, 127.3, 125.8, 125.51, 125.45, 125.3, 124.8, 123.4, 122.9, 122.7, 122.4, 122.1, 121.3, 120.2, 119.8, 119.5, 116.8, 114.0, 113.8, 111.7, 18.7. One ^{13}C resonance was not clearly located.

Synthesis of btp-C3. This complex was prepared according to general procedure using $[Ir(btp)_2(\mu\text{-}Cl)]_2$ (52 mg, 0.040 mmol), an excess of Na_2CO_3 (85 mg, 0.80 mmol), and **C3H** (22 mg, 0.079 mmol). The reaction was refluxed for 3 days. The product was obtained as a pale orange solid. Yield: 18 mg (26%). ^{1}H NMR (400 MHz, $CDCl_3$): δ = 8.81 (d, 1H, *J* = 5.8 Hz, Ar*H*), 8.77 (d, 1H, J = 5.8 Hz, Ar*H*), 8.11 (s, 1H, N=C*H*), 7.72–7.78 (m, 2H, Ar*H*), 7.63 (t, 2H, *J* = 8.4 Hz, Ar*H*), 7.41 (d, 1H, *J* = 8.1 Hz, Ar*H*), 7.27–7.32 (m, 2H, Ar*H*), 7.15 (dd, 1H, *J* = 8.0, 1.9 Hz, Ar*H*), 7.02–7.06 (m, 3H, Ar*H*), 6.95–6.98 (m, 1H, Ar*H*), 6.88

(t, 1H, *J* = 7.5 Hz, Ar*H*), 6.72–6.75 (m, 2H, Ar*H*), 6.62 (d, 1H, *J* = 7.9 Hz, Ar*H*), 6.45 (t, 1H, *J* = 7.1 Hz, Ar*H*), 6.29 (d, 1H, *J* = 7.8 Hz, Ar*H*), 6.11 (d, 2H, *J* = 9.9 Hz, Ar*H*), 6.04 (d, 1H, *J* = 8.5 Hz, Ar*H*), 5.96 (s, 1H, lactone C=C*H*), 2.19 (s, 3H, CH_3). $^{13}C\{^1H\}$ NMR (126 MHz, $CDCl_3$): δ = 166.5, 166.3, 165.8, 160.9, 160.7, 154.2, 152.8, 151.9, 149.9, 149.6, 149.3, 148.6, 146.7, 146.6, 142.6, 142.5, 138.4, 138.2, 136.3, 135.5, 135.2, 134.8, 125.7, 125.5, 125.2, 125.1, 124.9, 124.1, 123.7, 123.4, 122.8, 122.2, 120.7, 119.4, 119.12, 119.11, 118.9, 117.9, 117.3, 114.4, 114.0, 110.6, 18.7.

Synthesis of piq-C4. This complex was prepared according to general procedure using $[Ir(piq)_2(\mu\text{-}Cl)]_2$ (54 mg, 0.041 mmol), an excess of Na_2CO_3 (85 mg, 0.80 mmol), and **C4H** (24 mg, 0.082 mmol). The reaction was refluxed for 3 days. The product was obtained as a brown solid. Yield: 27 mg (36%). ^1H NMR (400 MHz, $CDCl_3$): δ = 8.95 (d, 1H, *J* = 6.4 Hz, Ar*H*), 8.92 (d, 1H, *J* = 9.7 Hz, Ar*H*), 8.51 (d, 1H, *J* = 6.4 Hz, Ar*H*), 8.34 (d, 1H, *J* = 8.7 Hz, Ar*H*), 8.22 (s, 1H, N=C*H*), 8.15 (d, 1H, *J* = 7.9 Hz, Ar*H*), 7.96 (d, 1H, *J* = 8.0 Hz, Ar*H*), 7.84–7.86 (m, 1H, Ar*H*), 7.73 (d, 1H, *J* = 8.0 Hz, Ar*H*) 7.65–7.70 (m, 2H, Ar*H*), 7.46 (t, 2H, *J* = 7.8 Hz, Ar*H*), 7.37 (d, 1H, *J* = 6.4 Hz, Ar*H*), 7.32 (t, 1H, *J* = 7.8 Hz, Ar*H*), 7.21 (t, 1H, *J* = 7.7 Hz, Ar*H*), 7.06 (d, 1H, *J* = 5.8 Hz, Ar*H*), 6.92 (q, 2H, *J* = 7.6 Hz, Ar*H*), 6.65–6.72 (m, 5H, Ar*H*), 6.48 (d, 1H, *J* = 6.8 Hz, Ar*H*), 6.39 (m, 2H, Ar*H*), 5.76–5.82 (m, 3H, Ar*H* + lactone C=C*H*), 2.02 (s, 3H, CH_3). The N*H* resonance was not clearly located, presumably due to overlap with aromatic C*H* resonances. $^{13}C\{^1H\}$ NMR (151 MHz, $CDCl_3$): δ = 169.6, 168.4, 166.9, 163.3, 161.0, 155.0, 153.9, 151.8, 150.7, 150.1, 147.3, 146.3, 141.0, 140.9, 137.2, 137.0, 135.0, 134.8, 133.8, 132.7, 130.9, 130.5, 130.2, 130.0, 129.9, 129.2, 127.9, 127.3, 127.2, 126.9, 126.7, 125.8, 125.6, 124.7, 124.4, 121.4, 121.2, 121.0, 120.4, 118.1, 114.2, 112.8, 111.3, 109.2, 98.7, 18.7.

Synthesis of pphen-C4. This complex was prepared in the glove box using $[Ir(pphen)_2(\mu\text{-}Cl)]_2$ (54 mg, 0.038 mmol), an excess of TEA (0.1 mL, 0.8 mmol), and **C4H** (24 mg, 0.082 mmol) in 5 mL of CH_2Cl_2. The reaction was stirred at room temperature under N_2 gas for 4 days. The remaining solid was filtered through a thin layer of alumina, using CH_2Cl_2 as an eluent to flush the product out and then further purified by precipitation from CH_2Cl_2/C_5H_{12} (1:5 v/v) to give a brown solid. Yield: 27 mg (36%). ^1H NMR (600 MHz, $CDCl_3$): δ = 9.40 (d, 1H, *J* = 7.9 Hz, Ar*H*), 9.14 (d, 1H, *J* = 8.2 Hz, Ar*H*), 8.67 (s, 1H, N=C*H*), 8.43 (d, 1H, *J* = 8.2 Hz, Ar*H*), 8.34 (s, 1H, Ar*H*), 8.17–8.21 (m, 4H, Ar*H*), 8.10 (s, 1H, Ar*H*), 7.85 (t, 1H, *J* = 7.6 Hz, Ar*H*), 7.77 (t, 1H, *J* = 7.7 Hz, Ar*H*), 7.50–7.54 (m, 6H, Ar*H*), 7.40 (s, 1H, N=C*H*), 7.17 (d, 1H, *J* = 7.7 Hz, Ar*H*), 7.08 (t, 1H, *J* = 7.6 Hz, Ar*H*), 7.01 (t, 1H, *J* = 7.5 Hz, Ar*H*), 6.73 (d, 2H, *J* = 7.7 Hz, Ar*H*), 6.61 (t, 1H, *J* = 7.4 Hz, Ar*H*), 6.46 (t, 1H, *J* = 7.9 Hz, Ar*H*), 6.41 (d, 1H, *J* = 7.7 Hz, Ar*H*), 6.28 (d, 1H, *J* = 8.6 Hz, Ar*H*), 6.14 (d, 1H, *J* = 7.6 Hz, Ar*H*), 5.92 (s, 1H, lactone C=C*H*), 5.89 (d, 2H, *J* = 8.0 Hz, Ar*H*), 5.78–5.83 (m, 2H, Ar*H*), 2.06 (s, 3H, CH_3). The N*H* resonance was not clearly located, presumably due to overlap with aromatic C*H* resonances. $^{13}C\{^1H\}$ NMR (151 MHz, $CDCl_3$): δ = 174.3, 173.3, 168.9, 165.7, 161.1,

153.7, 153.5, 152.1, 151.1, 150.3, 149.1, 148.2, 146.1, 143.0, 139.4, 134.9, 134.0, 133.8, 133.6, 133.3, 132.6, 131.5, 131.1, 131.0, 130.6, 130.1, 129.9, 129.5, 128.0,127.8, 127.3, 127.0, 126.7, 126.1, 126.0, 125.7, 124.7, 123.6, 123.4, 122.6, 122.5, 122.43, 122.38, 121.7, 121.1, 120.8, 120.6, 119.2, 112.9, 112.6, 111.2, 108.2, 100.0, 18.5. One ^{13}C resonance was not clearly located.

Synthesis of bt-C4. This complex was prepared according to general experimental preparation using $[Ir(bt)_2(\mu\text{-}Cl)]_2$ (52 mg, 0.040 mmol), an excess of TEA (0.1 mL, 0.8 mmol), and **C4H** (24 mg, 0.082 mmol). The reaction was refluxed for 3 days. The product was obtained as an orange solid. Yield: 24 mg (33%). ^1H NMR (400 MHz, $CDCl_3$): δ = 8.61–8.64 (m, 1H, Ar*H*) 8.10 (s, 1H, N=C*H*), 7.97 (d, 1H, *J* = 7.9 Hz, Ar*H*), 7.84 (dd, 1H, *J* = 8.1, 1.2 Hz, Ar*H*), 7.65 (dd, 1H, *J* = 7.6, 1.2 Hz, Ar*H*), 7.54 – 7.56 (m, 1H, Ar*H*), 7.36 – 7.48 (m, 5H, Ar*H*), 7.17 (ddd, 1H, J = 8.7, 6.9, 1.9 Hz, Ar*H*), 6.86 – 6.94 (m, 4H, Ar*H*), 6.67 – 6.74 (m, 3H, Ar*H*), 6.61 (t, 2H, *J* = 3.4 Hz, Ar*H*), 6.28 – 6.32 (m, 2H, Ar*H*), 6.02 (d, 1H, *J* = 1.3 Hz, lactone C=C*H*) 5.84 (dd, 1H, *J* = 8.7, 2.3 Hz, Ar*H*), 5.79 (d, 1H, *J* = 2.4 Hz, Ar*H*), 2.28 (d, 3H, *J* = 1.1 Hz, CH_3). The N*H* resonance was not clearly located, presumably due to overlap with aromatic C*H* resonances. $^{13}C\{^1H\}$ NMR (151 MHz, $CDCl_3$): δ = 181.1, 180.5, 167.9, 165.0, 160.9, 154.4, 152.4, 152.2, 151.2, 150.49, 150.47, 146.5, 142.6, 141.9, 135.4, 134.8, 134.7, 133.3, 131.5, 131.4, 131.3, 130.4, 128.6, 127.4, 126.4, 125.73, 125.69, 125.3, 124.7, 124.3, 123.0, 122.4, 122.2, 121.9, 121.4, 119.4, 118.9, 114.0, 113.4, 111.6, 109.5, 99.22, 18.7.

Synthesis of btp-C4. This complex was prepared according to general experimental preparation using $[Ir(btp)_2(\mu\text{-}Cl)]_2$ (52 mg, 0.040 mmol), an excess of TEA (0.1 mL, 0.8 mmol) and **C4H** (24 mg, 0.082 mmol). The reaction was refluxed for 5 days. The product was obtained as an orange solid. Yield: 23 mg (32%). ^1H NMR (400 MHz, $CDCl_3$): δ = 8.93 (d, 1H, *J* = 5.8 Hz, Ar*H*), 8.56 (d, 1H, *J* = 5.7 Hz, Ar*H*), 8.25 (s, 1H, N=C*H*), 7.67–7.75 (m, 2H, Ar*H*), 7.61 (t, 1H, *J* = 9.2 Hz, Ar*H*), 7.38 (t, 1H, *J* = 7.7 Hz, Ar*H*), 7.30 (t, 1H, *J* = 7.9 Hz, Ar*H*), 7.06–7.17 (m, 3H, Ar*H*), 7.02 (q, 2H, *J* = 6.5 Hz, Ar*H*), 6.94 (t, 1H, *J* = 6.5 Hz, Ar*H*), 6.88 (t, 2H, *J* = 8.3 Hz, Ar*H*), 6.76 (d, 1H, *J* = 8.6 Hz, Ar*H*), 6.72 (t, 1H, *J* = 7.6 Hz, Ar*H*), 6.47 (t, 1H, *J* = 7.3 Hz, Ar*H*), 6.29 (d, 2H, *J* = 8.0 Hz, Ar*H*), 6.06 (s, 1H, lactone C=C*H*), 6.00 (d, 1H, *J* = 8.1 Hz, Ar*H*), 5.94 (d, 1H, *J* = 2.4 Hz, Ar*H*), 5.78 (dd, 1H, *J* = 8.7, 2.3 Hz, Ar*H*), 2.33 (s, 3H, CH_3). The N*H* resonance was not clearly located, presumably due to overlap with aromatic C*H* resonances. $^{13}C\{^1H\}$ NMR (151 MHz, $CDCl_3$): δ = 166.4, 166.1, 165.7, 162.9, 161.1, 154.4, 152.4, 150.6, 150.0, 149.9, 149.4, 146.7, 146.2, 144.6, 142.8, 142.5, 138.3, 137.8, 137.3, 136.7, 135.2, 134.9, 125.6, 125.4, 124.90, 124.88, 124.6, 124.2, 123.7, 123.1, 122.8, 119.9, 119.3, 117.60, 117.57, 114.7, 113.4, 111.6, 110.1, 98.6, 18.7. Two ^{13}C resonances were not clearly located.

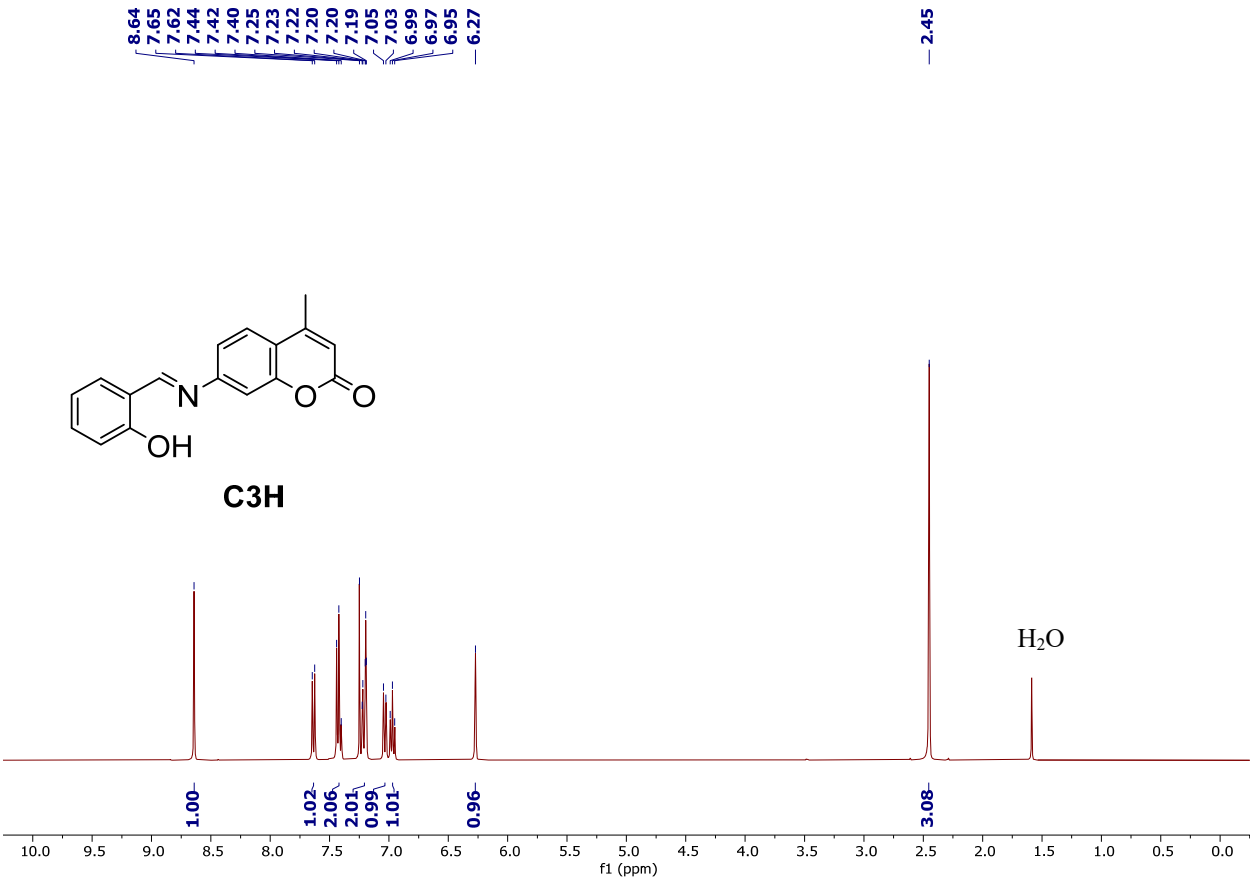

Fig. S1. ^{1}H NMR spectrum of **C3H** recorded at 400 MHz in $CDCl_3$.

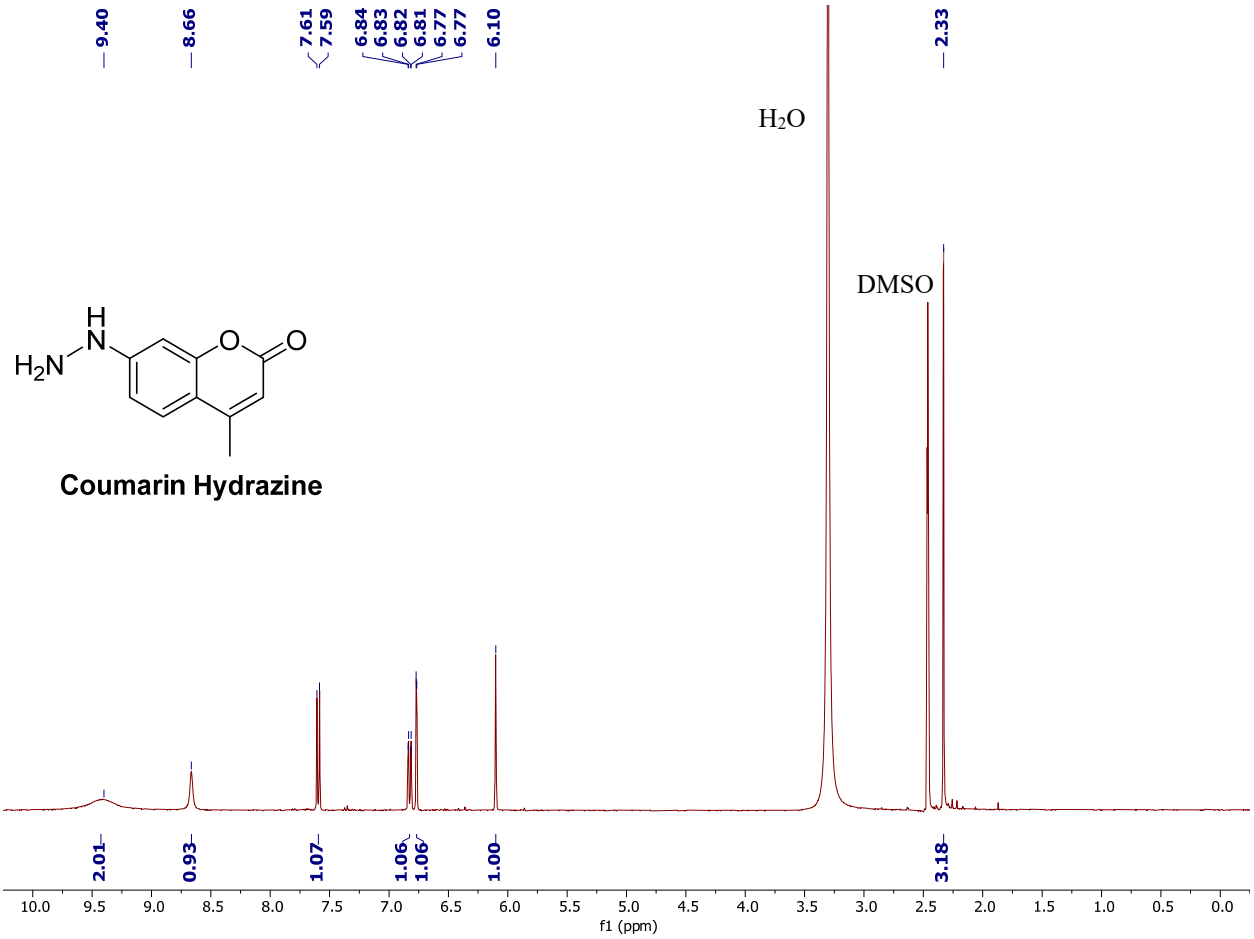

Fig. S2. ^{1}H NMR spectrum of **Coumarin Hydrazine** recorded at 400 MHz in DMSO-d_6.

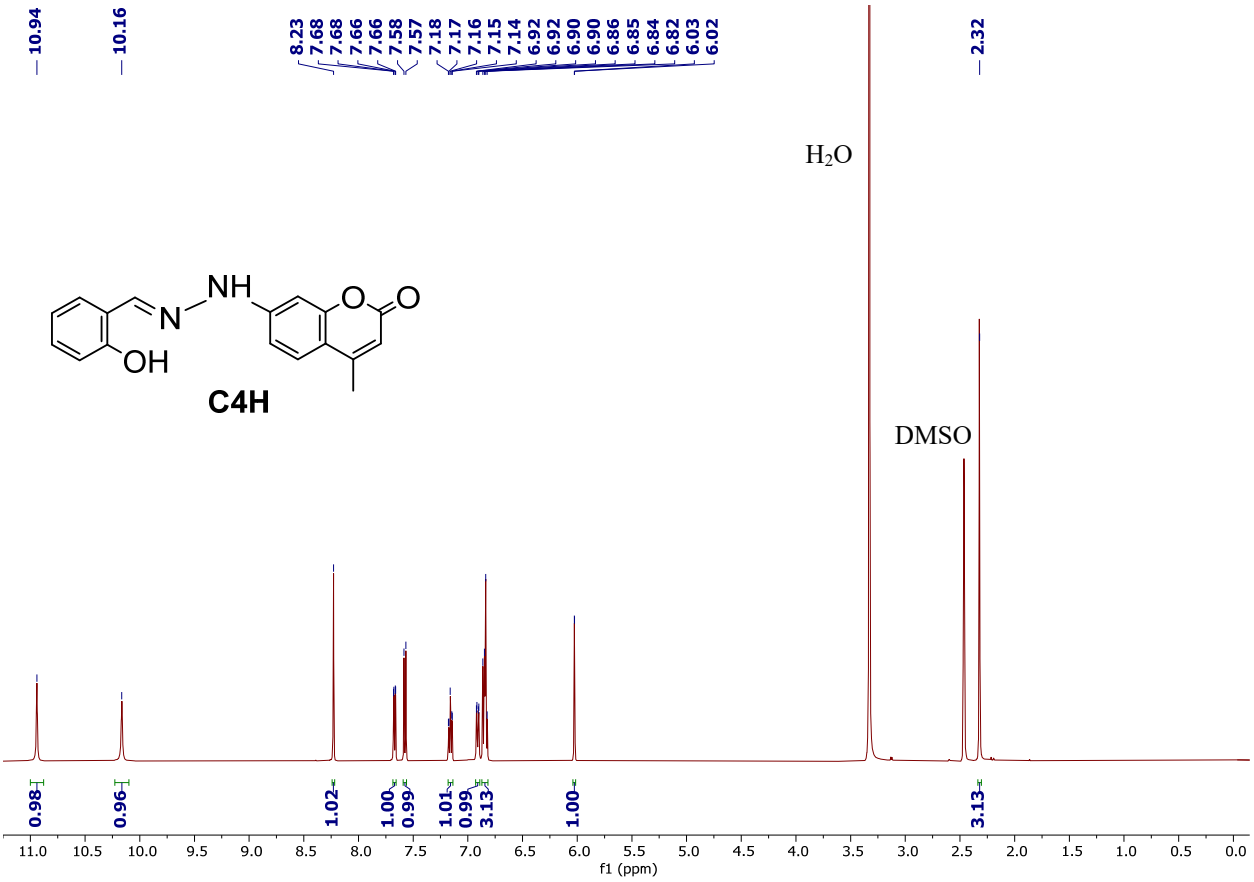

Fig. S3. ^{1}H NMR spectrum of **C4H** recorded at 500 MHz in DMSO-d_6.

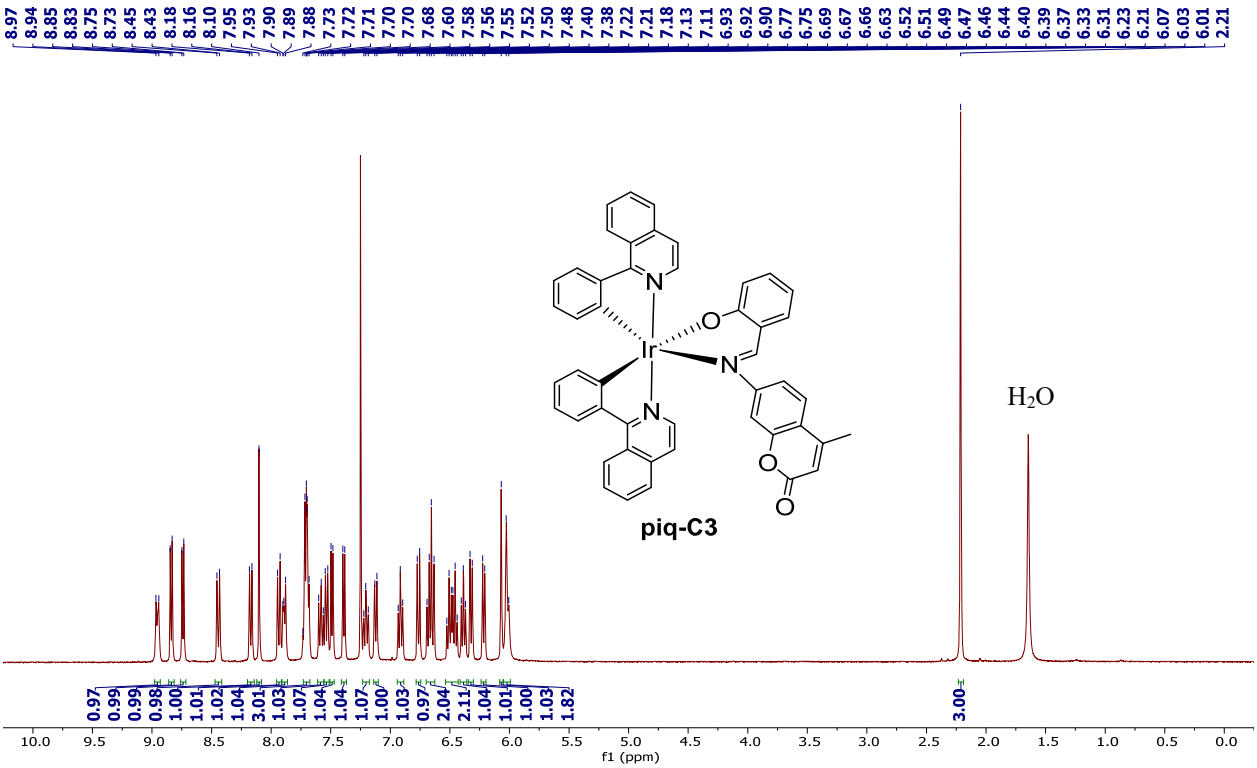

Fig. S4. ^{1}H NMR spectrum of complex **piq-C3** recorded at 400 MHz in $CDCl_3$.

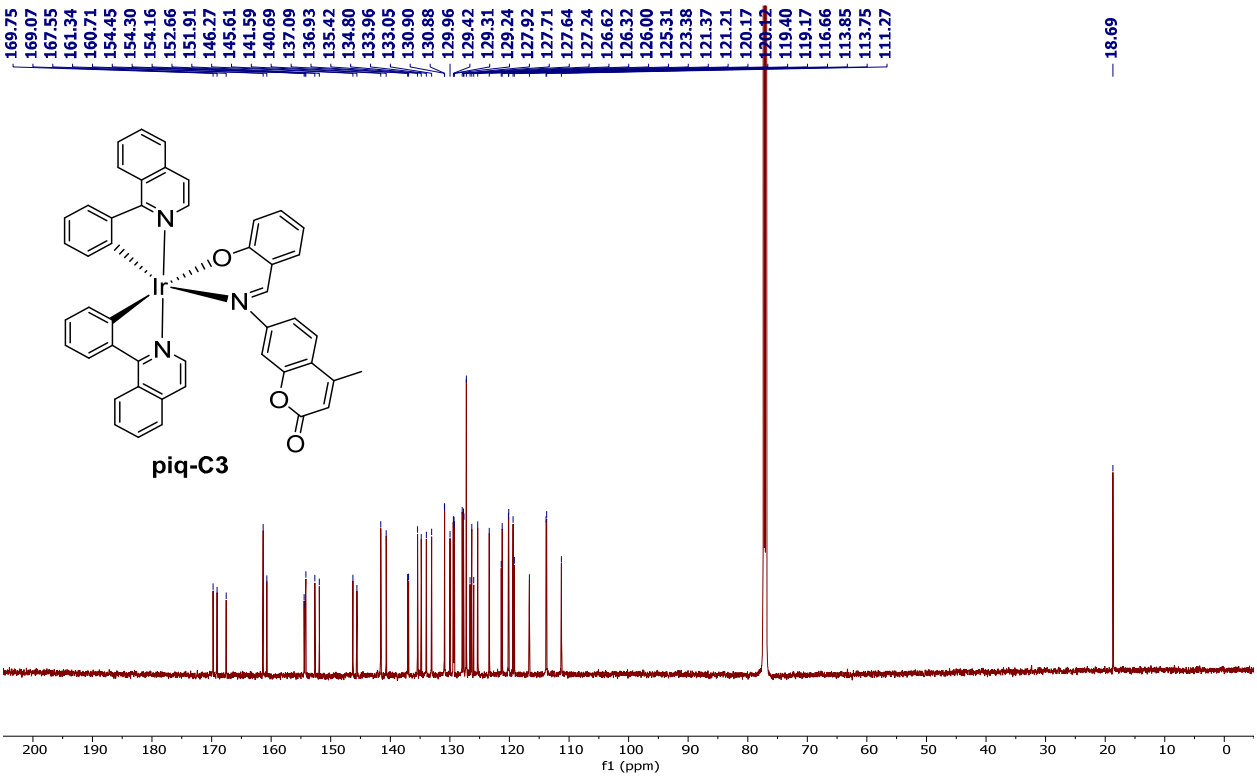

Fig. S5. $^{13}C\{^{1}H\}$ NMR spectrum of complex **piq-C3** recorded at 151 MHz in $CDCl_3$.

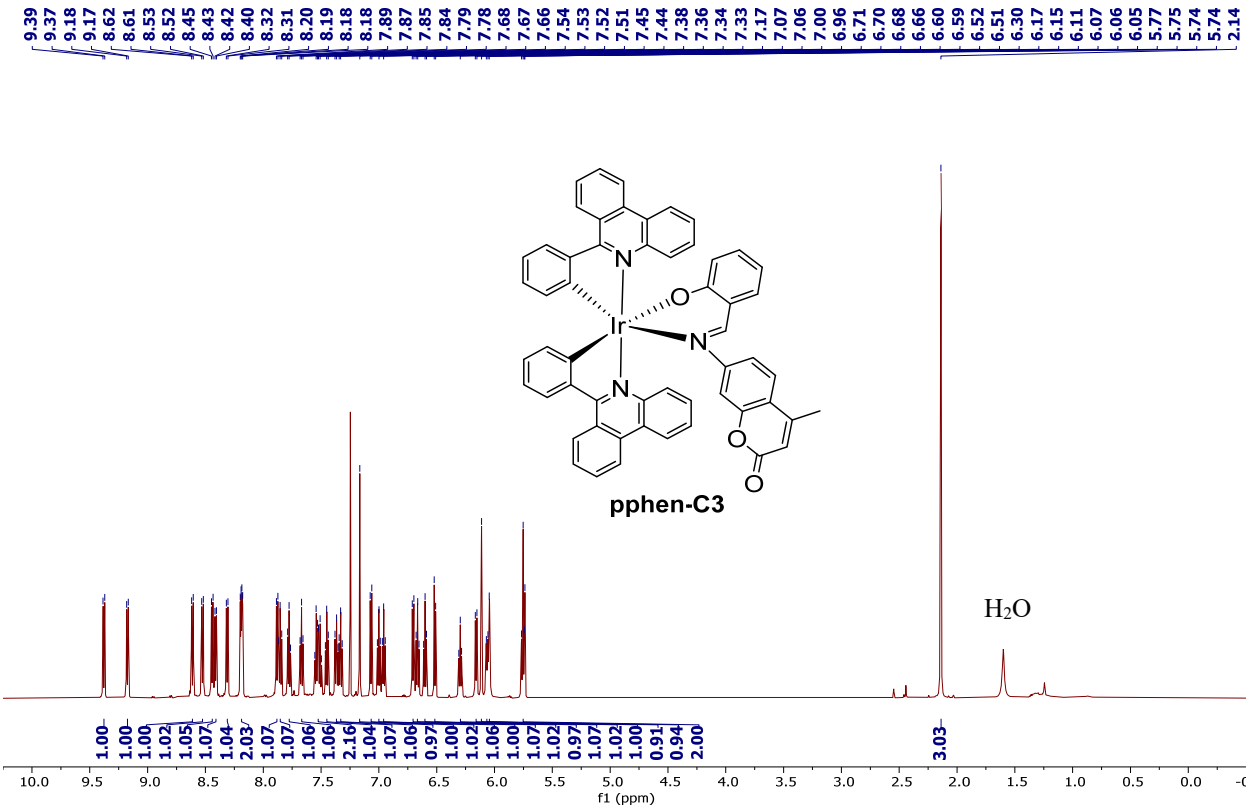

Fig. S6. ^{1}H NMR spectrum of complex **pphen-C3** recorded at 600 MHz in $CDCl_3$.

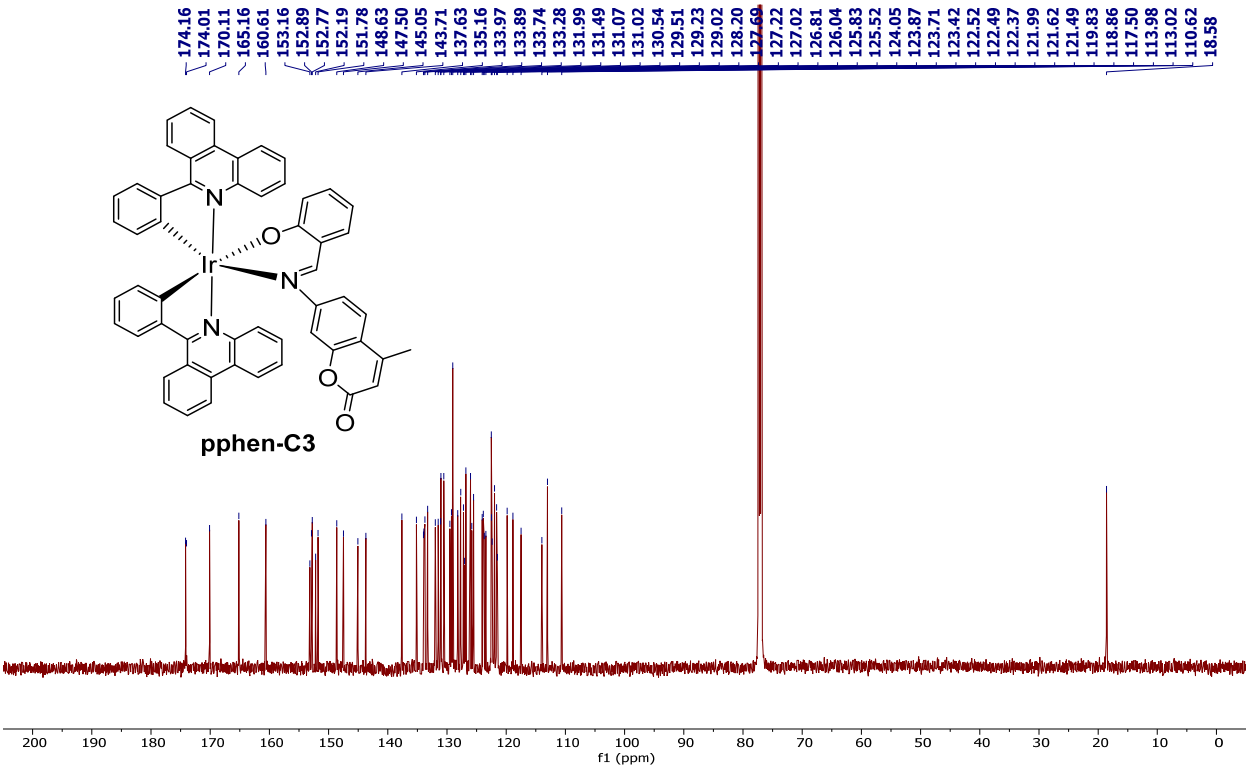

Fig. S7. $^{13}C\{^{1}H\}$ NMR spectrum of complex **pphen-C3** recorded at 151 MHz in $CDCl_3$.

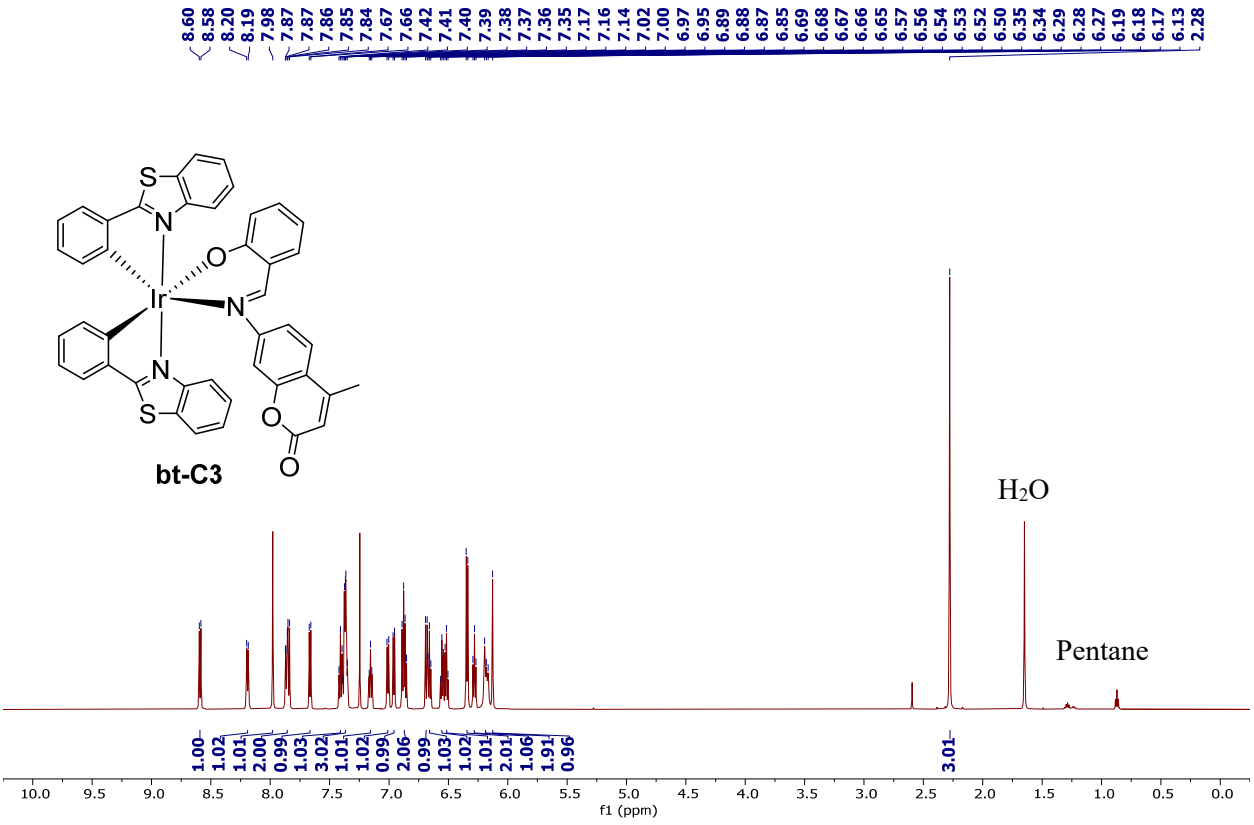

Fig. S8. ^{1}H NMR spectrum of complex **bt-C3** recorded at 600 MHz in $CDCl_3$.

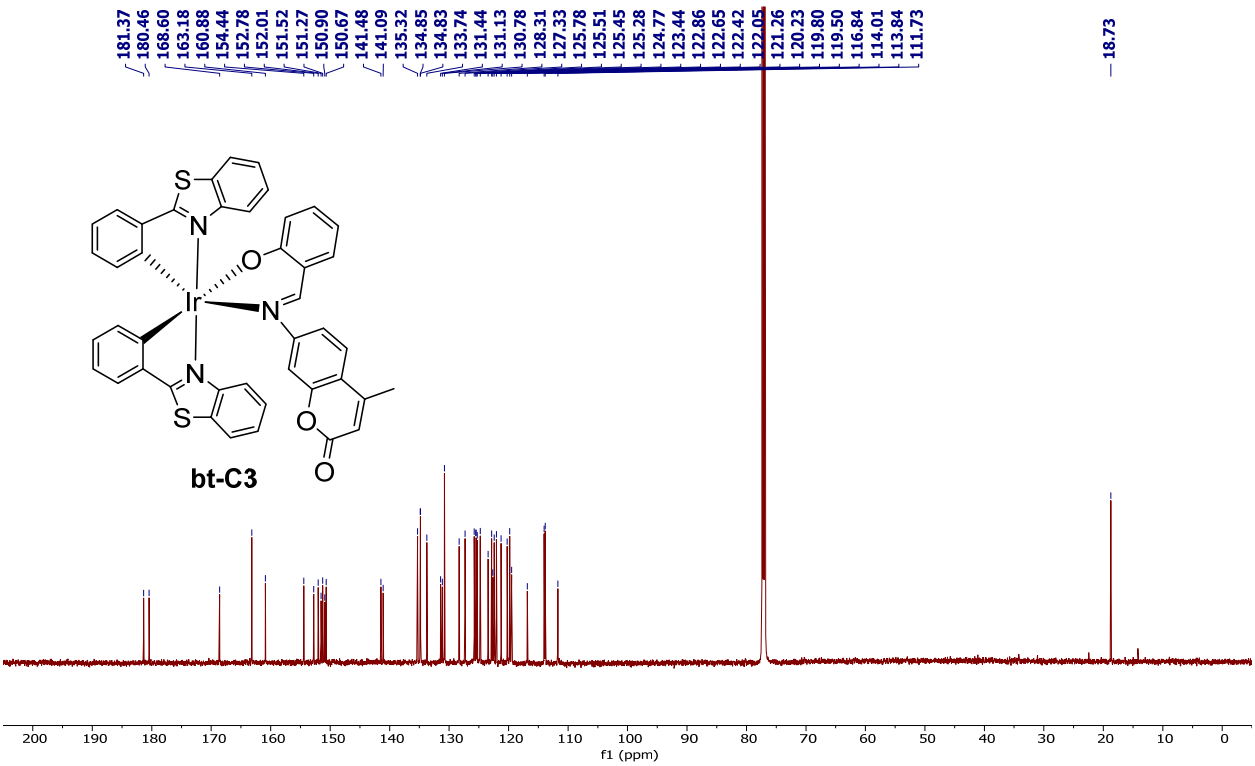

Fig. S9. $^{13}C\{^{1}H\}$ NMR spectrum of complex **bt-C3** recorded at 151 MHz in $CDCl_3$.

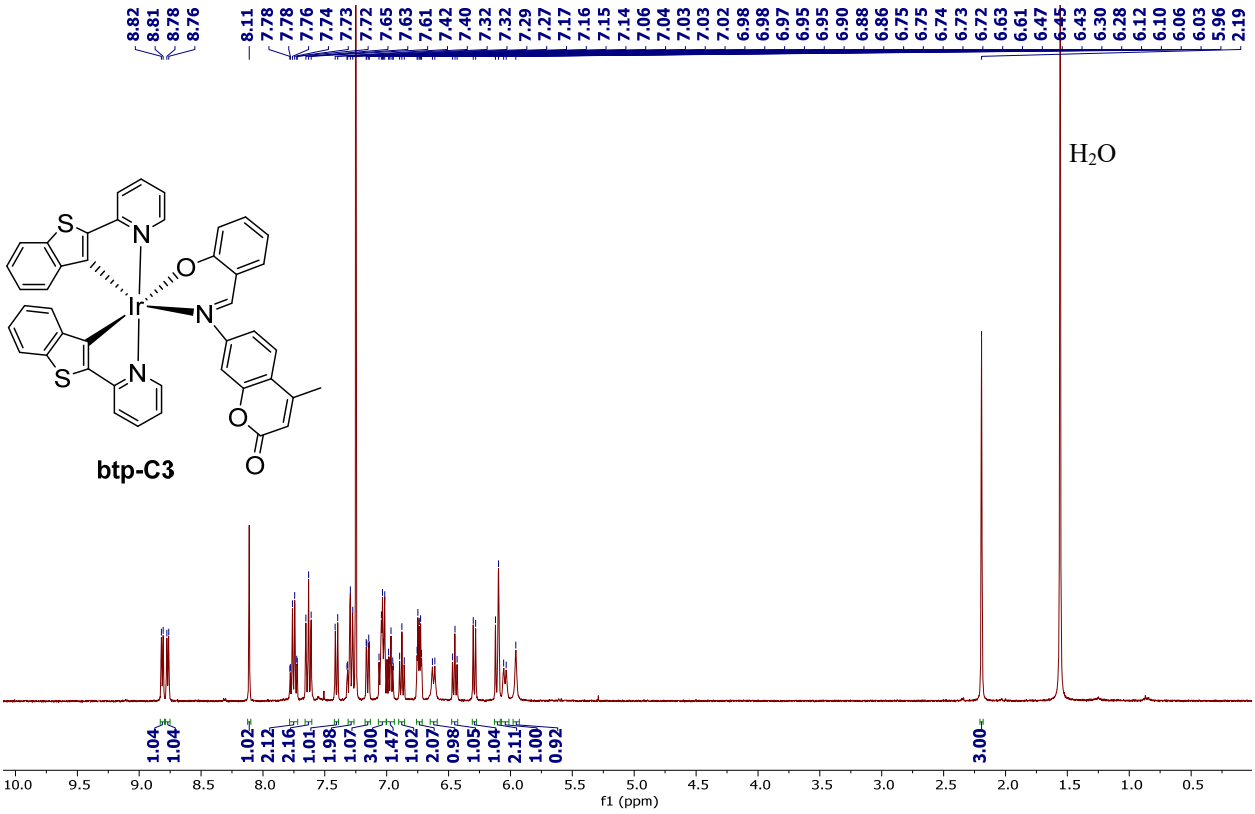

Fig. S10. ^{1}H NMR spectrum of complex **btp-C3** recorded at 400 MHz in $CDCl_3$.

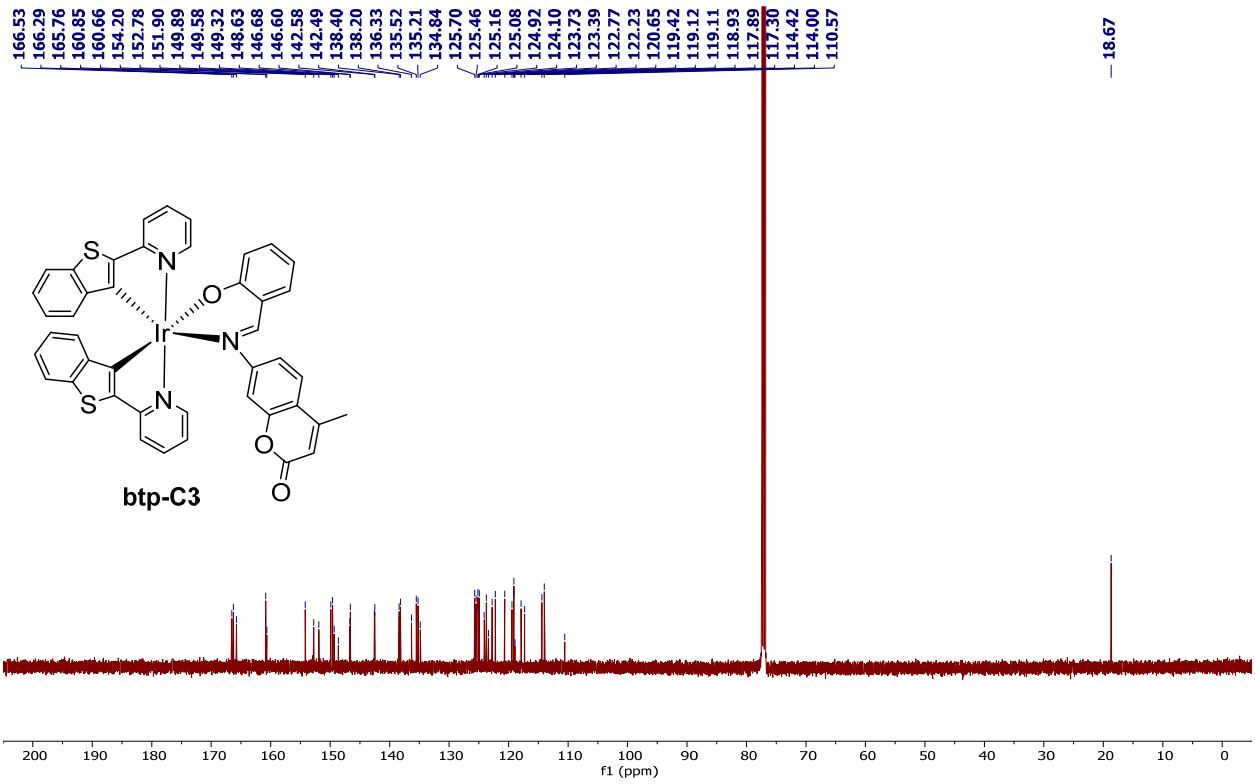

Fig. S11. $^{13}C\{^{1}H\}$ NMR spectrum of complex **btp-C3** recorded at 126 MHz in $CDCl_3$.

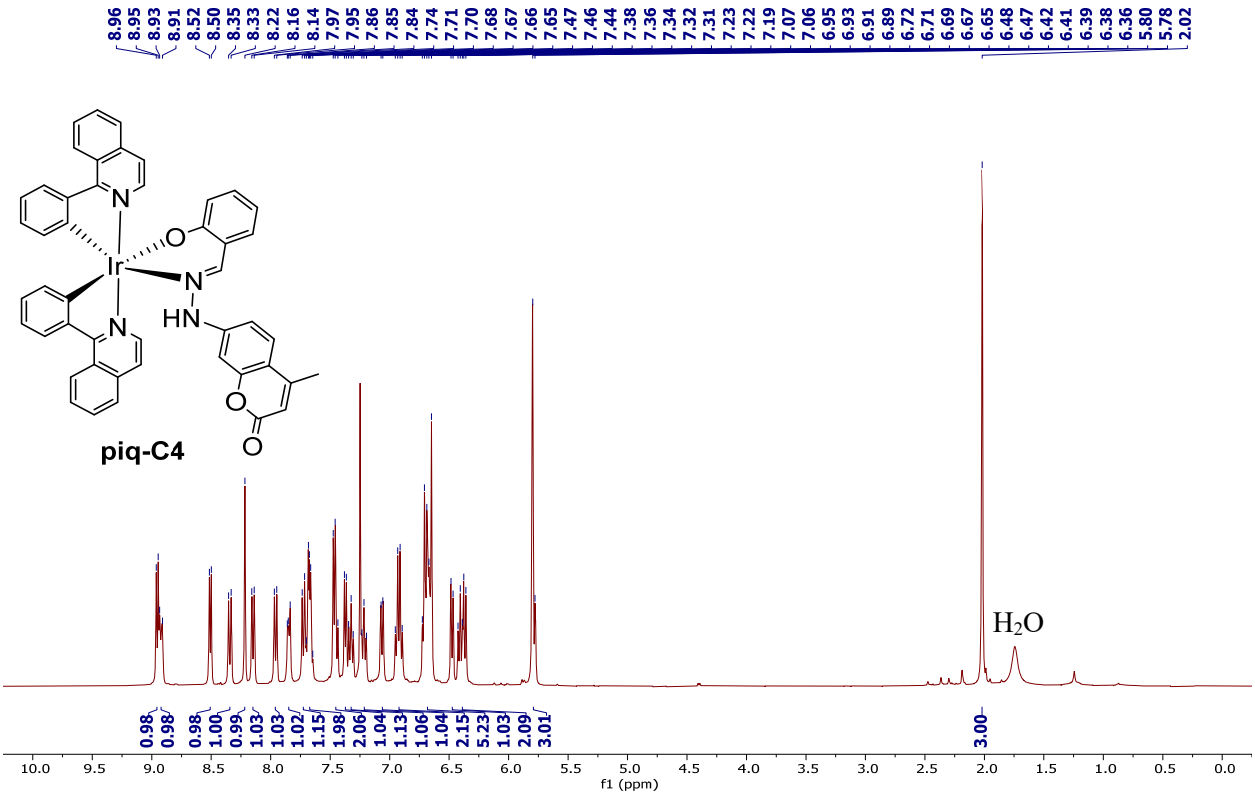

Fig. S12. ^{1}H NMR spectrum of complex **piq-C4** recorded at 400 MHz in $CDCl_3$.

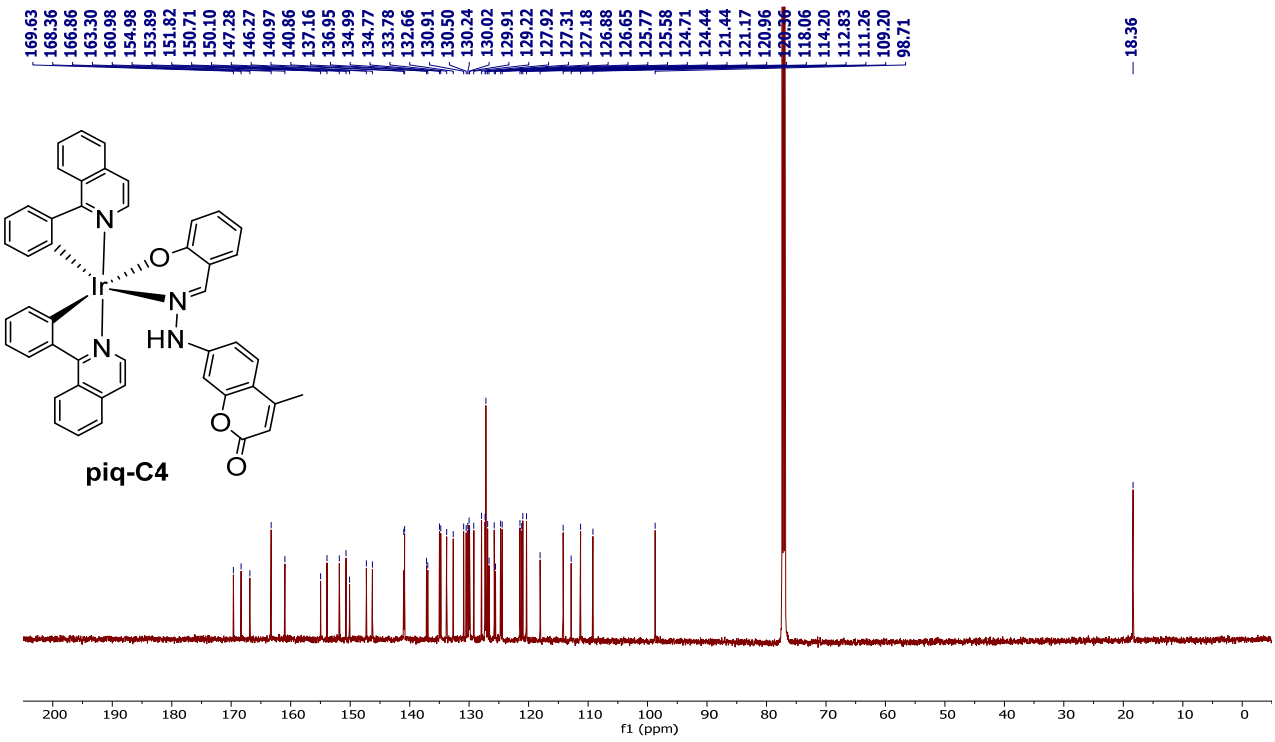

Fig. S13. $^{13}C\{^{1}H\}$ NMR spectrum of complex **piq-C4** recorded at 151 MHz in $CDCl_3$.

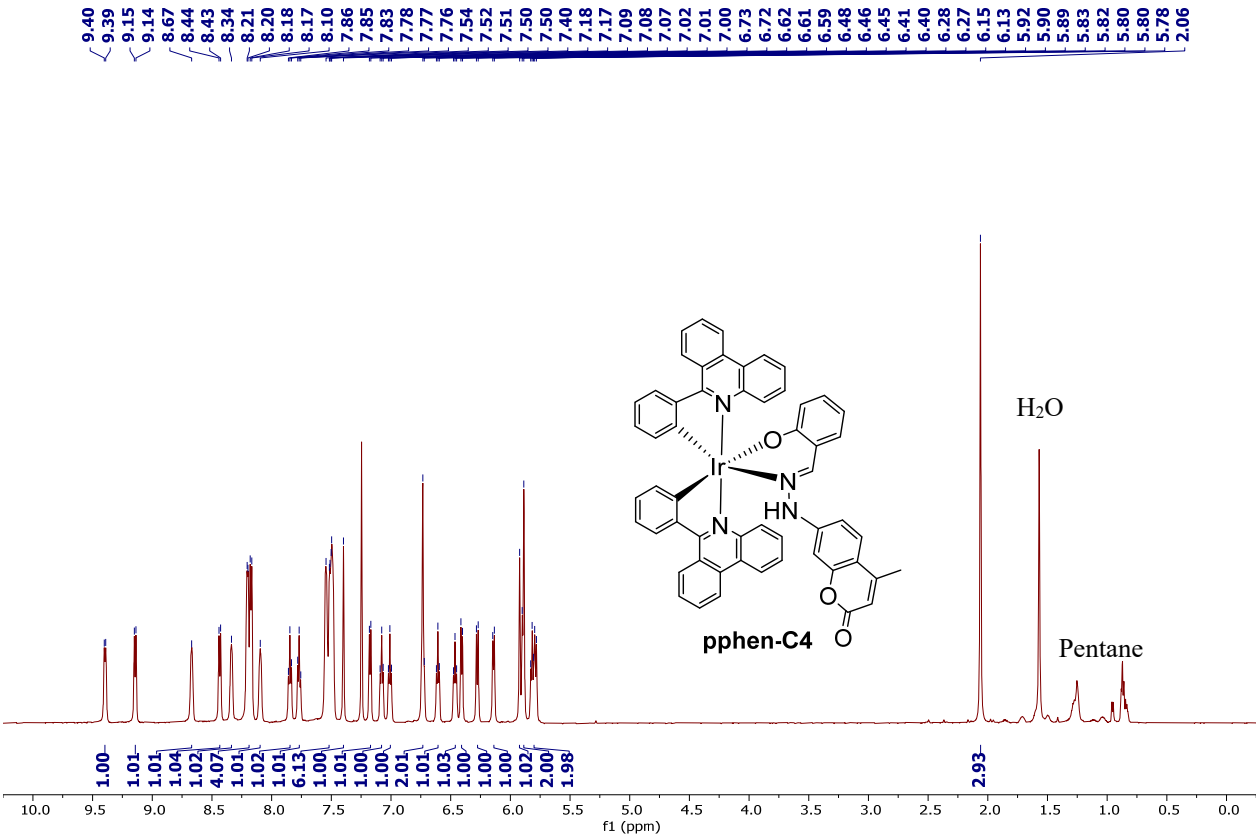

Fig. S14. ^{1}H NMR spectrum of complex **pphen-C4** recorded at 600 MHz in $CDCl_3$.

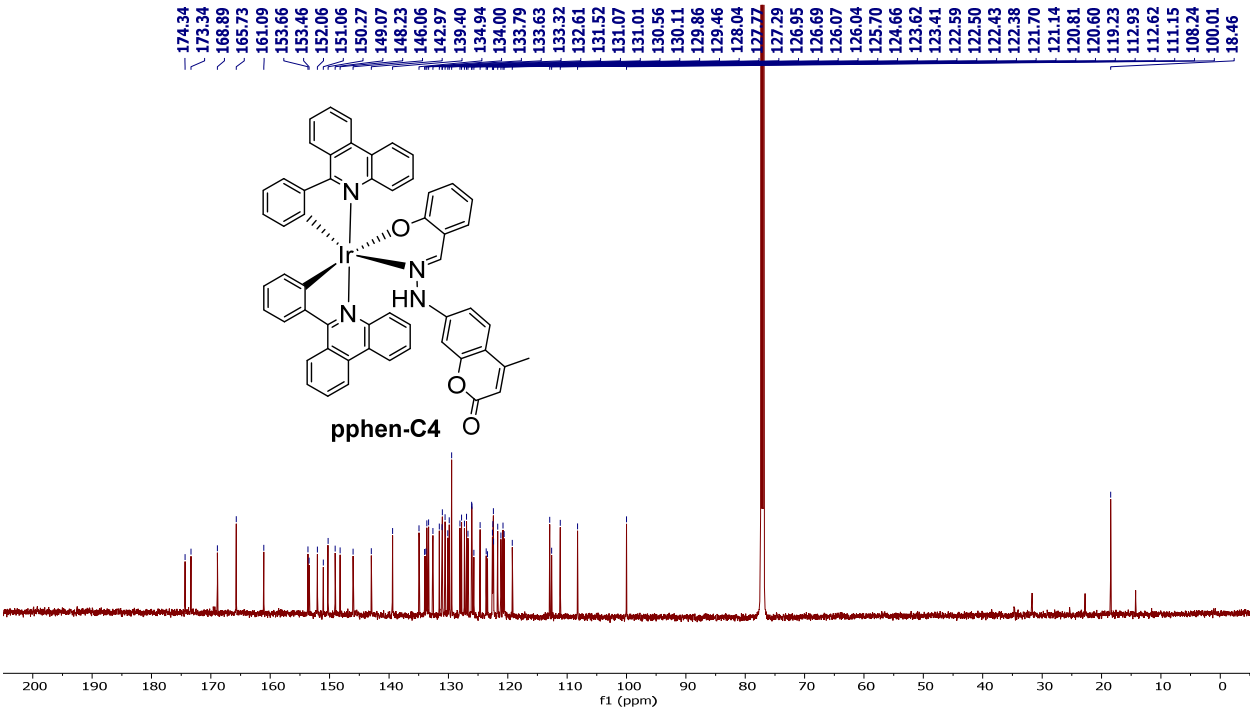

Fig. S15. $^{13}C\{^{1}H\}$ NMR spectrum of complex **pphen-C4** recorded at 151 MHz in $CDCl_3$.

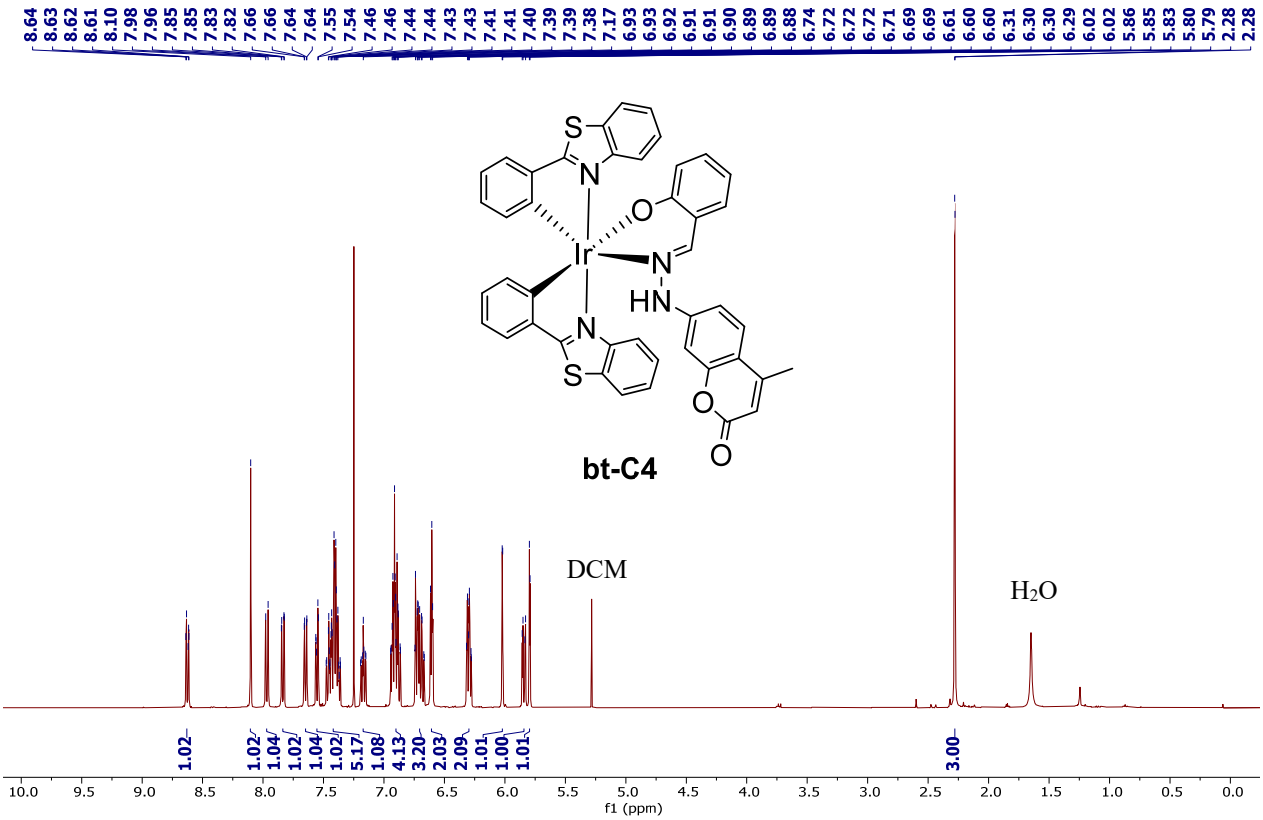

Fig. S16. ^{1}H NMR spectrum of complex **bt-C4** recorded at 400 MHz in $CDCl_3$.

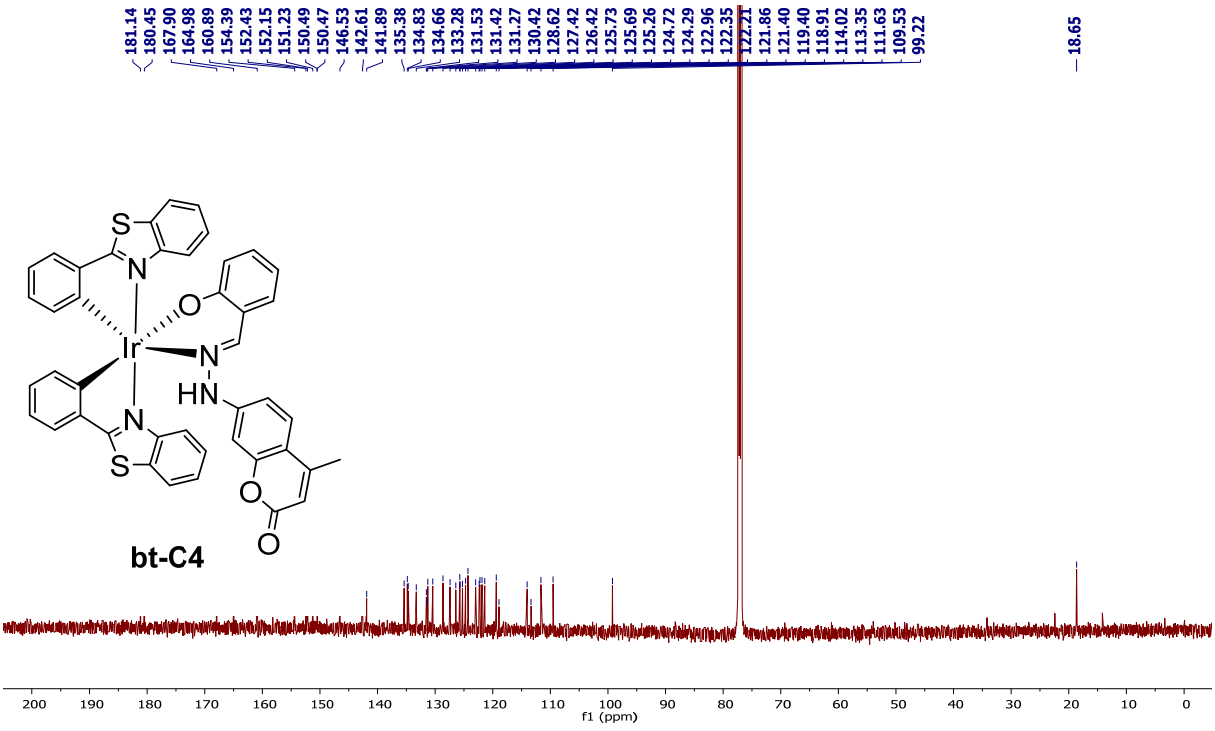

Fig. S17. $^{13}C\{^{1}H\}$ NMR spectrum of complex **bt-C4** recorded at 151 MHz in $CDCl_3$.

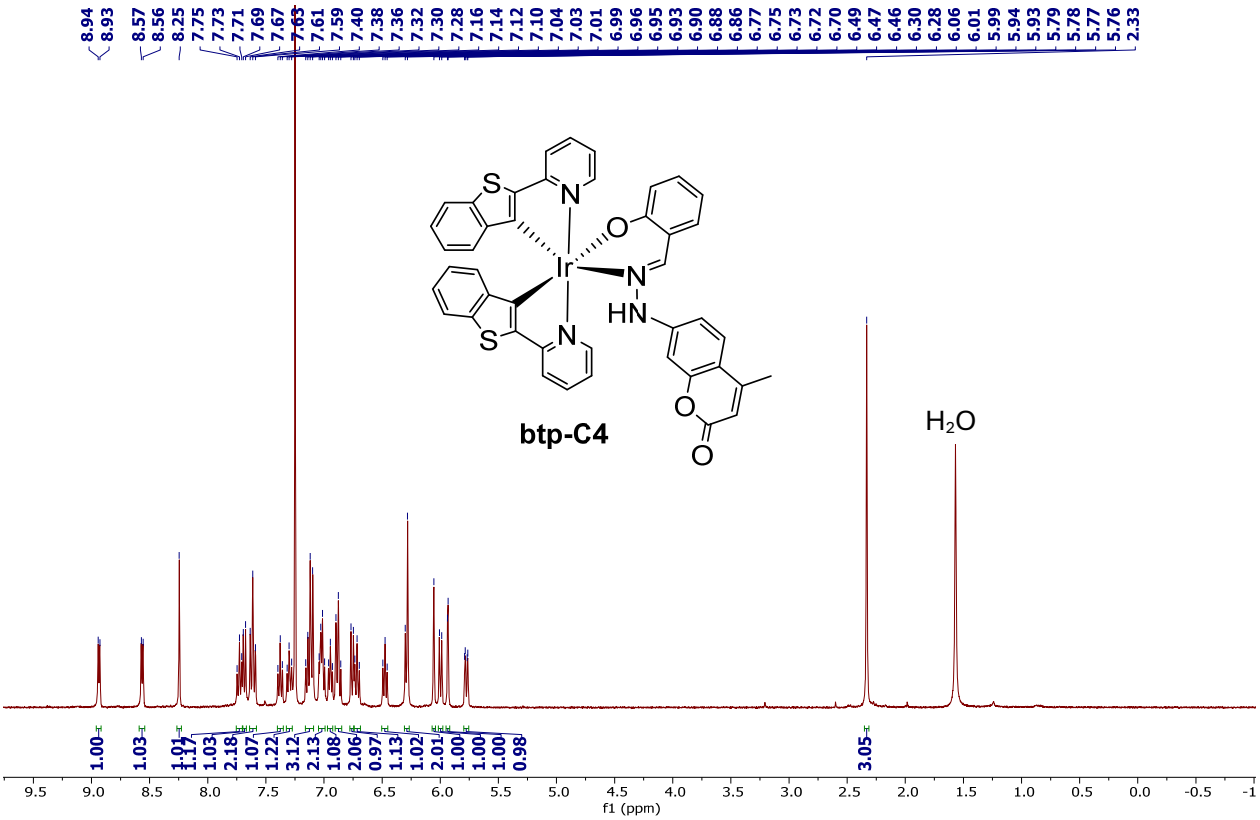

Fig. S18. ^{1}H NMR spectrum of complex **btp-C4** recorded at 400 MHz in $CDCl_3$.

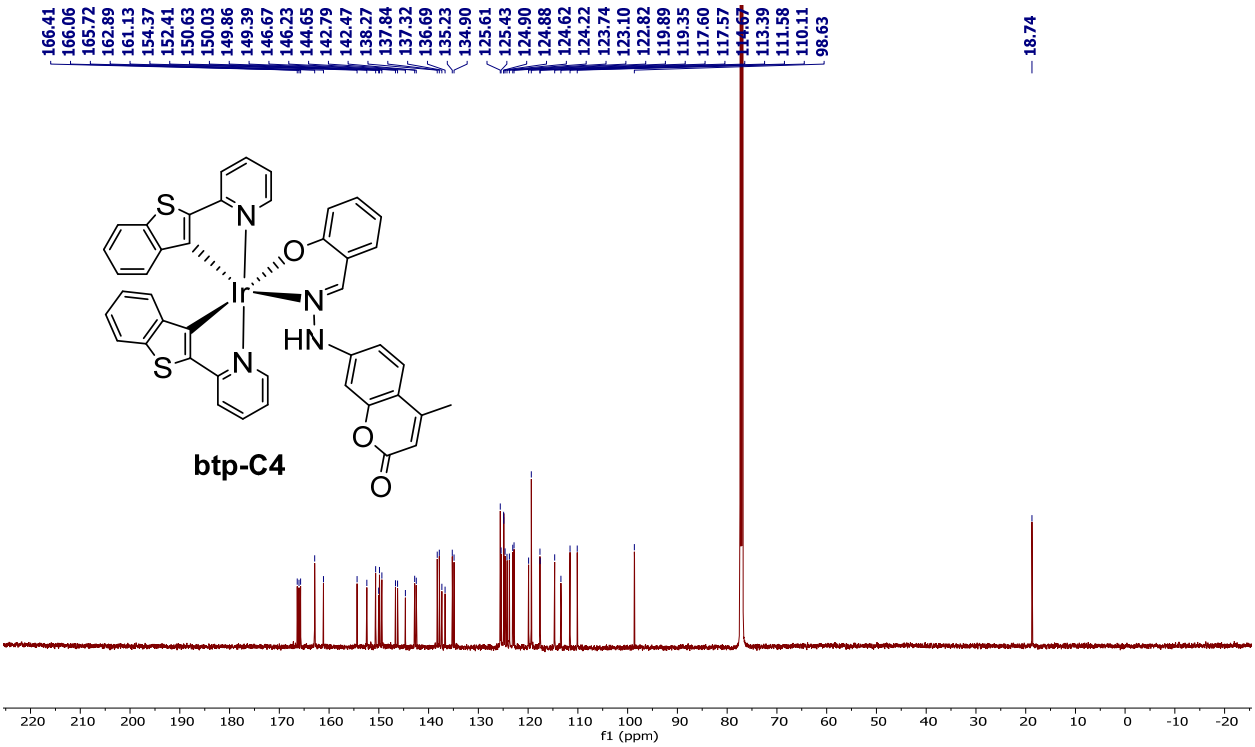

Fig. S19. $^{13}C\{^{1}H\}$ NMR spectrum of complex **btp-C4** recorded at 151 MHz in $CDCl_3$.

Table S1. Crystallographic summary for **bt-C3**, **btp-C4**, and **piq-C3**.

	bt-C3·CH_2Cl_2	**btp-C4**	**piq-C3**
CCDC	c	2355725	2355726
Crystal data			
Chemical formula	$C_{44}H_{30}Cl_2IrN_3O_3S_2$	$C_{43}H_{29}IrN_4O_3S_2$	$C_{47}H_{32}IrN_3O_3$
M_r	975.93	906.02	878.95
Crystal system, space group	Monoclinic, $P2_1/c$	Monoclinic, $P2_1$/n	Monoclinic, $P2_1/n$
a, b, c (Å)	11.1502(17), 24.938(4), 14.546(2)	15.564(2), 14.1664(19), 15.798(2)	17.873(5), 10.022(3), 19.645(6)
α, β, γ (°)	90, 100.657(2), 90	90, 100.365(2), 90	90, 100.260(4), 90
V (Å^3)	3975.0(10)	3426.4(8)	3462.6(18)
Z	4	4	4
μ (mm^{-1})	3.64	4.07	3.91
Crystal size (mm)	0.38 × 0.3 × 0.2	0.30 × 0.30 × 0.20	0.32 × 0.17 × 0.11
Data collection			
T_{min}, T_{max}	0.490, 0.746	0.608, 0.746	0.497, 0.746
No. of measured, independent and observed [I>2σ(I)]	24800, 9149, 8335	20884, 7877, 7046	20396, 7606, 5846
R_{int}	0.028	0.033	0.061
$(\sin \theta/\lambda)_{max}$ (Å^{-1})	0.651	0.651	0.641
Refinement			
$R[F^2 > 2\sigma(F^2)]$, $wR(F^2)$, S	0.026, 0.061, 1.03	0.025, 0.062, 1.03	0.043, 0.091, 1.01
No. of reflections	9149	7877	7606
No. of parameters	497	482	488
No. of restrains	0	1	0
$\Delta\rho_{max}$, $\Delta\rho_{min}$ (eÅ^{-3})	1.40, −0.90	1.79, −1.25	2.00, −1.21

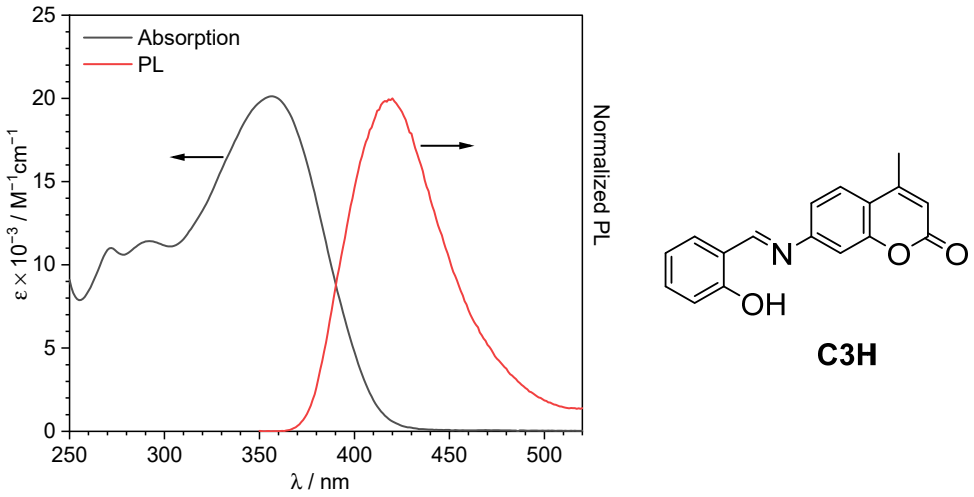

Fig. S20. Overlaid UV–vis absorption (black solid line) and photoluminescence (red solid line) spectra of coumarin **C3H** recorded at 293 K in dichloromethane, λ_{ex} = 310 nm.

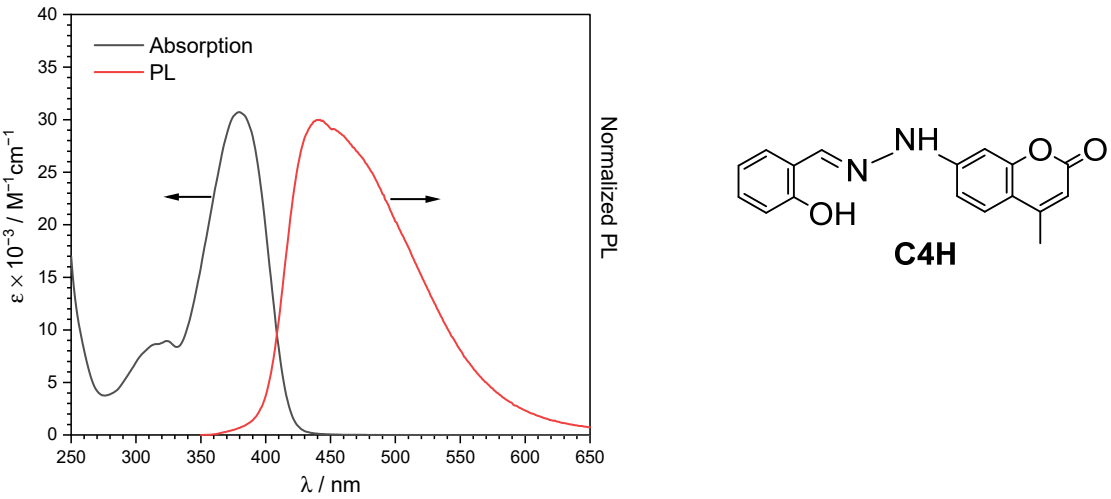

Fig. S21. Overlaid UV-vis absorption (black solid line) and photoluminescence (red solid line) spectra of coumarin **C4H** recorded at 293 K in dichloromethane (stock solution is prepared in DMSO to promote solubility), λ_{ex} = 310 nm.

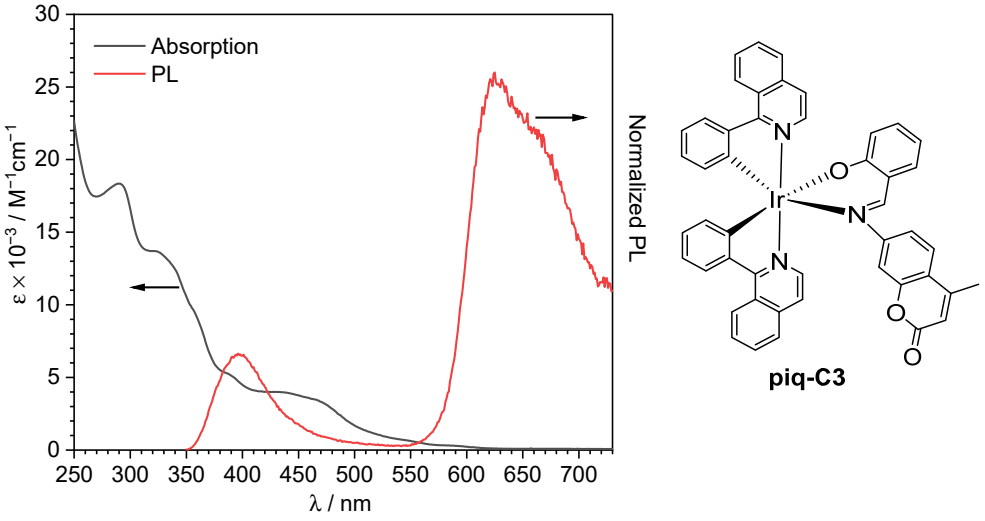

Fig. S22. Overlaid UV–vis absorption (black solid line) and photoluminescence (red solid line) spectra of **piq-C3** recorded at 293 K in CH_2Cl_2, λ_{ex} = 310 nm.

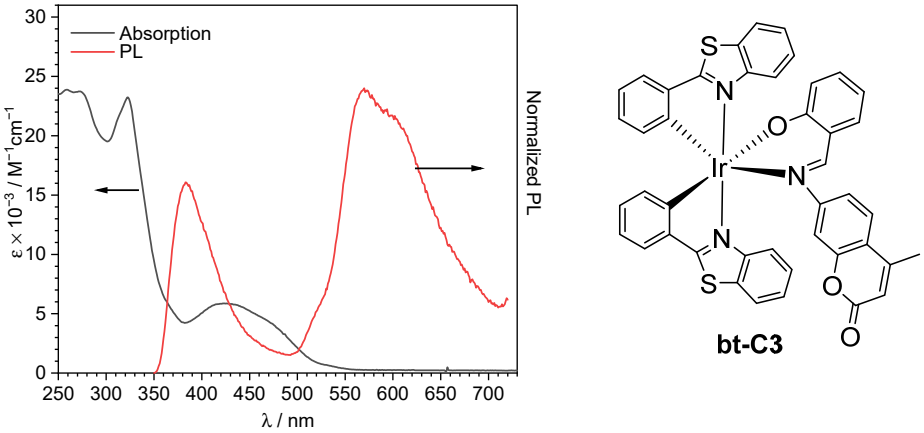

Fig. S23. Overlaid UV-vis absorption (black solid line) and photoluminescence (red solid line) spectra of **bt-C3**, recorded at 293 K in CH_2Cl_2, λ_{ex} = 310 nm.

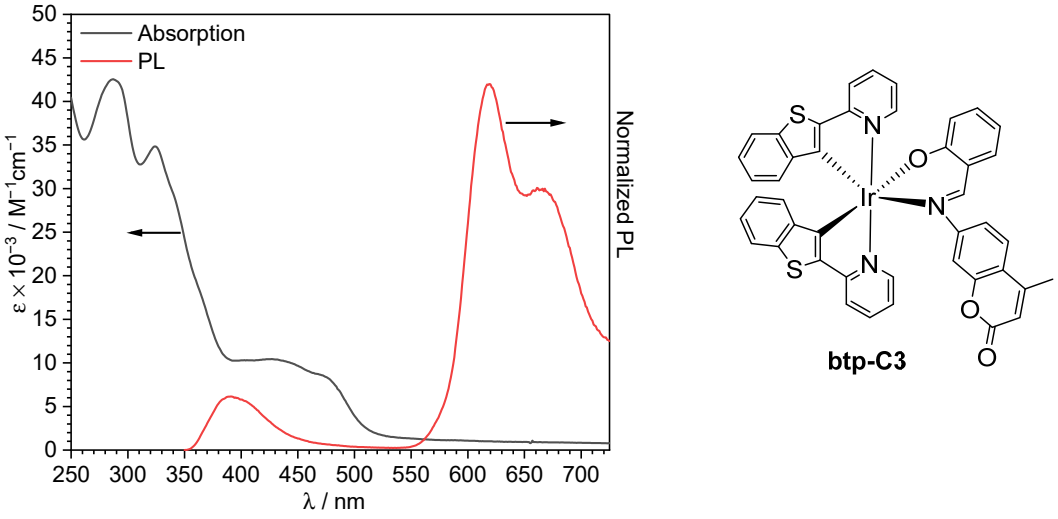

Fig. S24. Overlaid UV-vis absorption (black solid line) and photoluminescence (red solid line) spectra of **btp-C3**, recorded at 293 K in CH_2Cl_2, λ_{ex} = 310 nm. The PL spectrum was truncated to avoid detection of the second-order harmonic of the coumarin-centered fluorescence band.

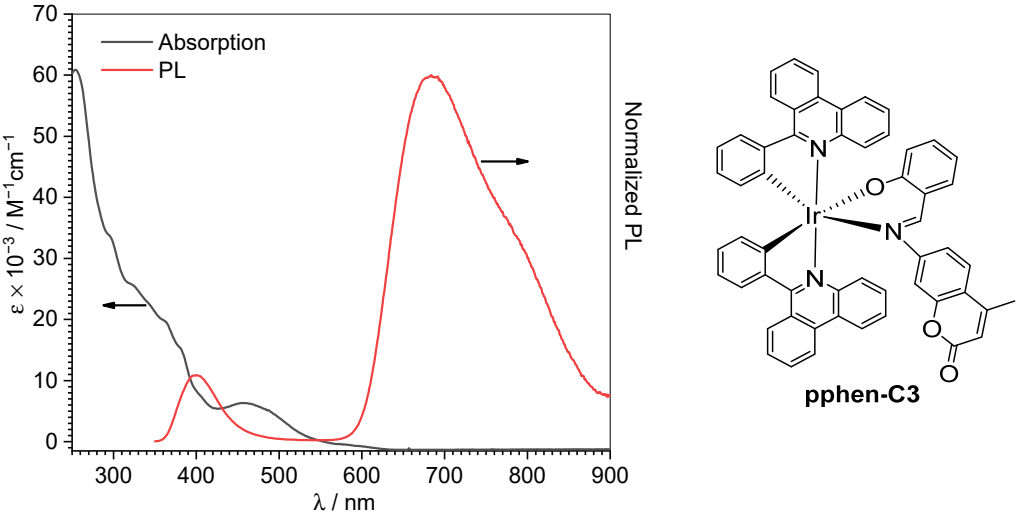

Fig. S25. Overlaid UV-vis absorption (black solid line) and photoluminescence (red solid line) spectra of **pphen-C3**, recorded at 293 K in CH_2Cl_2, λ_{ex} = 310 nm.

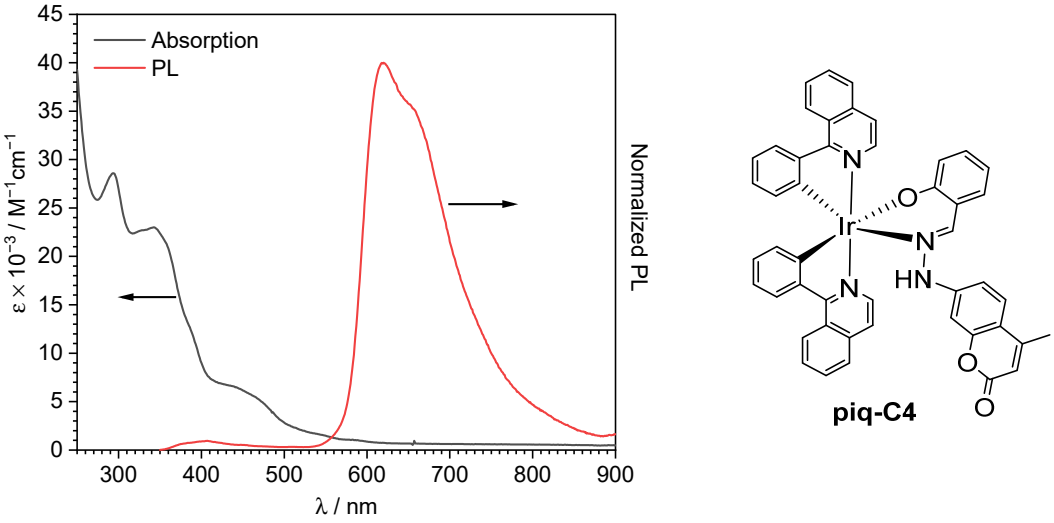

Fig. S26. Overlaid UV-vis absorption (black solid line) and photoluminescence (red solid line) spectra of **piq-C4**, recorded at 293 K in CH_2Cl_2, λ_{ex} = 310 nm.

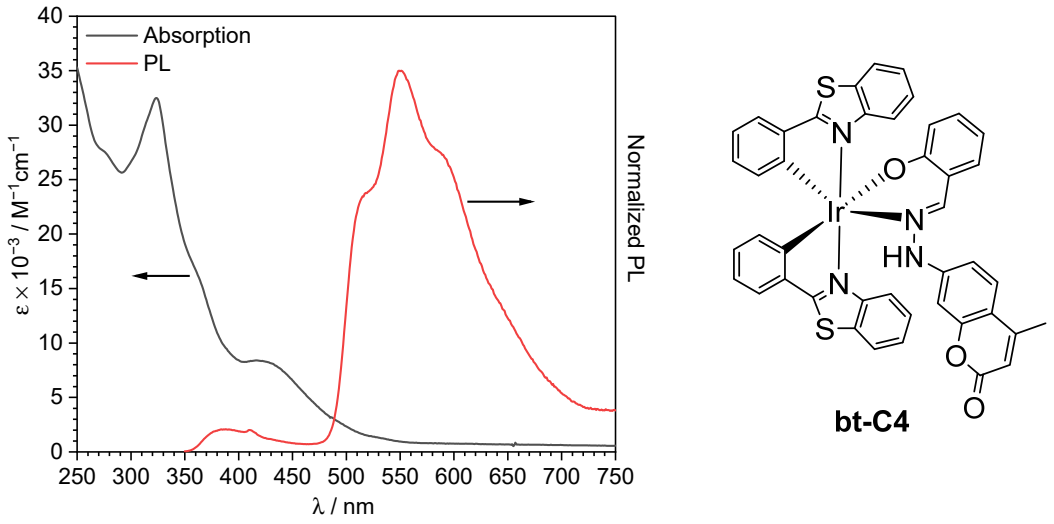

Fig. S27. Overlaid UV-vis absorption (black solid line) and photoluminescence (red solid line) spectra of **bt-C4**, recorded at 293 K in CH_2Cl_2, λ_{ex} = 310 nm.

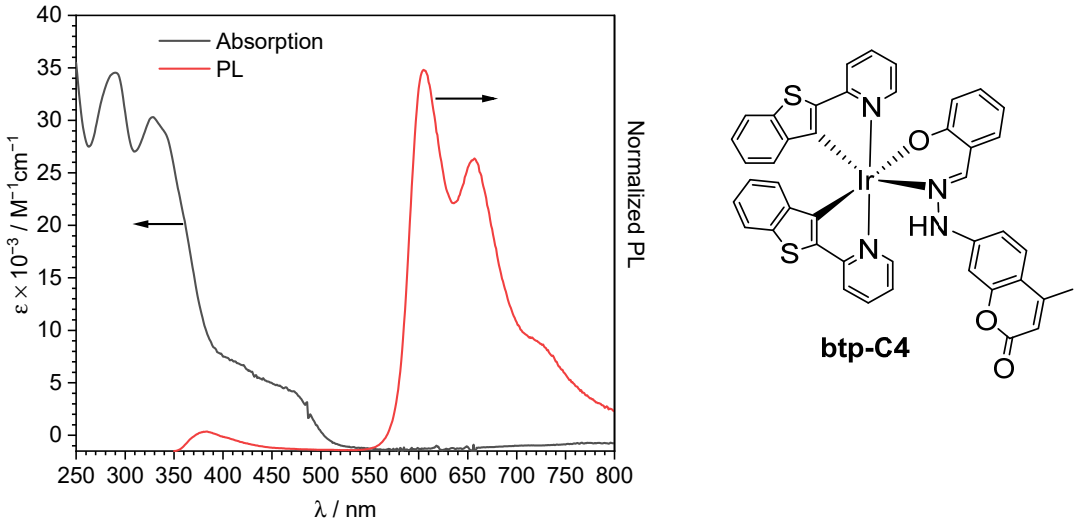

Fig. S28. Overlaid UV-vis absorption (black solid line) and photoluminescence (red solid line) spectra of **btp-C4**, recorded at 293 K in CH_2Cl_2, λ_{ex} = 310 nm.

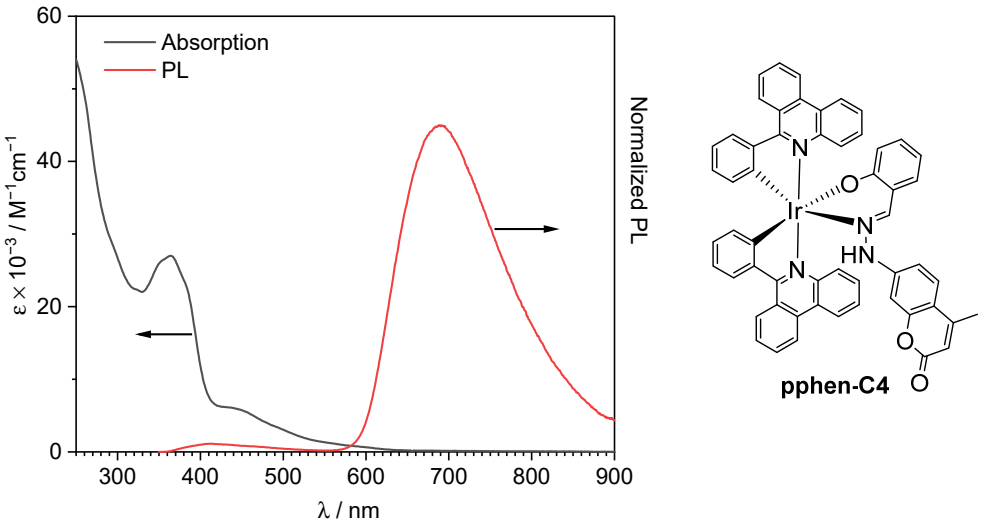

Fig. S29. Overlaid UV-vis absorption (black solid line) and photoluminescence (red solid line) spectra of **pphen-C4**, recorded at 293 K in CH_2Cl_2, λ_{ex} = 310 nm.

Table S2. Summary of photophysical data for the salicylaldimine-coumarin precursors **C3H** and **C4H**, recorded in dichloromethane at 293 K.

	Absorption λ / nm ($\varepsilon \times 10^{-3}$ / $M^{-1}cm^{-1}$)	λ_{em}[a] / nm	Φ_{Flu}[a]	τ[b] / ns	(k_r[c] $\times 10^{-6}$ / s^{-1})/ (k_{nr}[c] $\times 10^{-8}$ / s^{-1})
C3H	272 (11) 292 (11), 357 (20)	420	0.34%	2.7	1.3/3.7
C4H	325 (8.9), 380 (31)	442	8.8%[d]	2.3[d]	38/4.0

[a] excitation wavelength at 310 nm. [b] excitation wavelength at 330 nm. [c] $k_r = \Phi_{Flu}/\tau$ and $k_{nr} = (1-\Phi_{Flu})/\tau$. [d] stock solution is prepared by DMSO to promote solubility.

Table S3. Additional photophysical data for the iridium-coumarin complexes, recorded in dichloromethane at 293 K.

	Absorption λ / nm ($\varepsilon \times 10^{-3}$ / $M^{-1}cm^{-1}$)	($k_{r,Phos}$[a] × 10^{-5} / s^{-1})/ ($k_{nr,Phos}$[a] × 10^{-5} / s^{-1})
piq-C3	290 (18), 315 (14) 355 (sh), 391 (5.0), 430 (4)	0.74/43
bt-C3	323 (23), 424 (5.9)	0.13/1.5
btp-C3	287 (43), 323 (35), 353 (sh), 427 (10)	0.016/2.8
pphen-C3	292 (34), 322 (sh), 458 (6.3)	1.9/27
piq-C4	293 (28), 342 (23), 425 (6.8)	2.0/22
bt-C4	324 (32), 355 (18) 417 (8.4)	0.12/0.95
btp-C4	290 (34), 329 (30), 345 (sh)	0.034/2.1
pphen-C4	364 (27), 437 (6.1)	2.3/13

[a] $k_{r,Phos} = \Phi_{Phos}/\tau_{Phos}$ and $k_{nr} = (1-\Phi_{Phos})/\tau_{Phos}$.

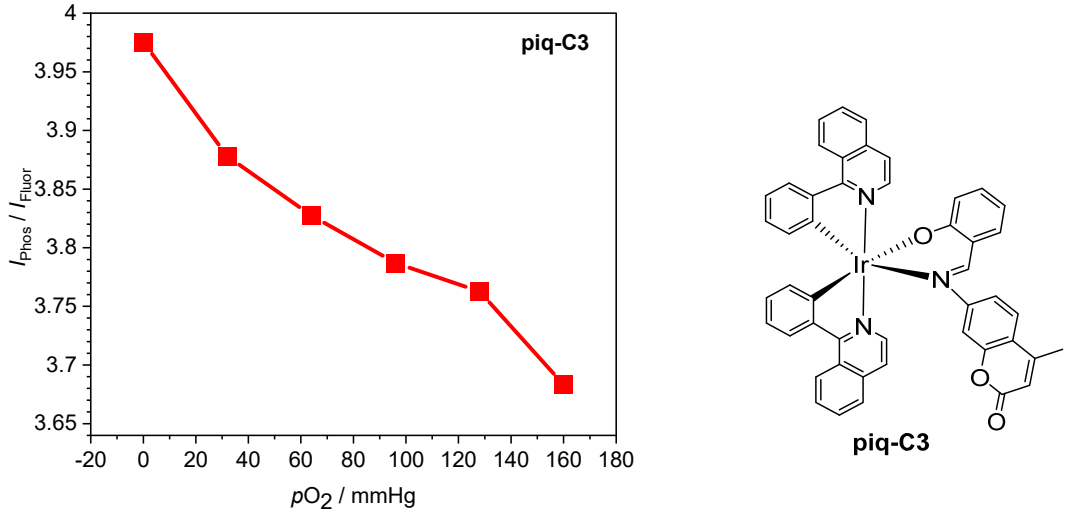

Fig. S30. Plot of the ratio of phosphorescence to fluorescence intensity of **piq-C3**, recorded as a function of oxygen partial pressure (pO_2). The luminescence intensities were rerecorded as the maximum intensity values of the long-wavelength phosphorescence (I_{Phos}) and short-wavelength fluorescence (I_{Fluor}) bands.

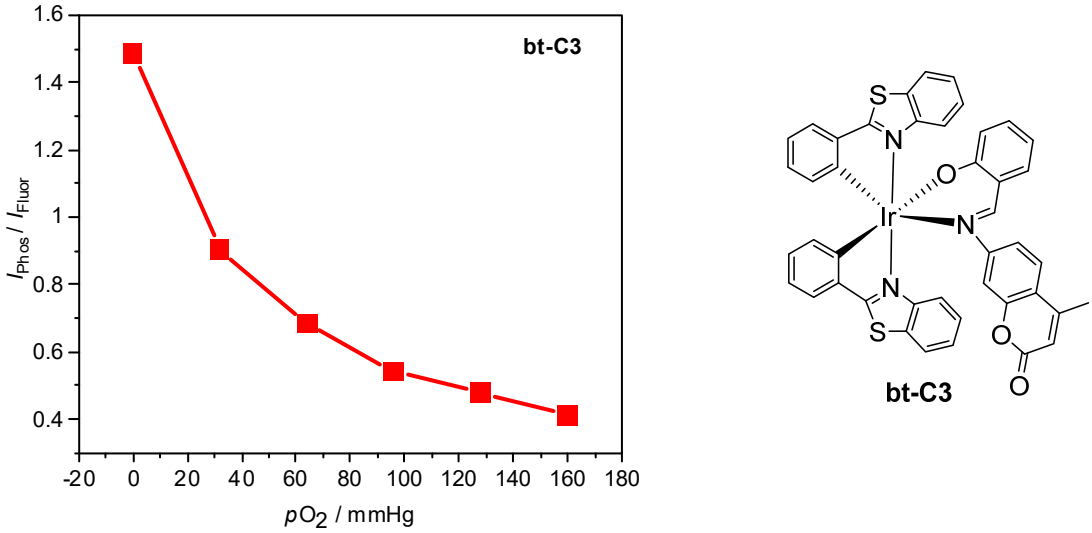

Fig. S31. Plot of the ratio of phosphorescence to fluorescence intensity of **bt-C3**, recorded as a function of oxygen partial pressure (pO_2). The luminescence intensities were rerecorded as the maximum intensity values of the long-wavelength phosphorescence (I_{Phos}) and short-wavelength fluorescence (I_{Fluor}) bands.

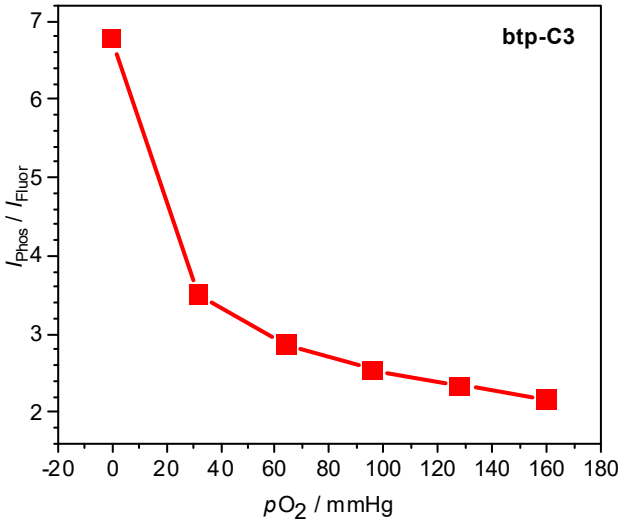

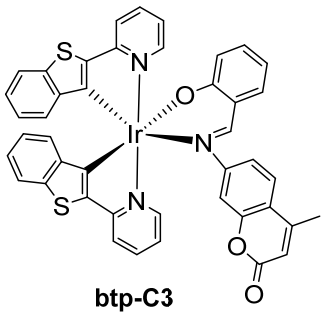

Fig. S32. Plot of the ratio of phosphorescence to fluorescence intensity of **btp-C3**, recorded as a function of oxygen partial pressure (pO_2). The luminescence intensities were rerecorded as the maximum intensity values of the long-wavelength phosphorescence (I_{Phos}) and short-wavelength fluorescence (I_{Fluor}) bands.

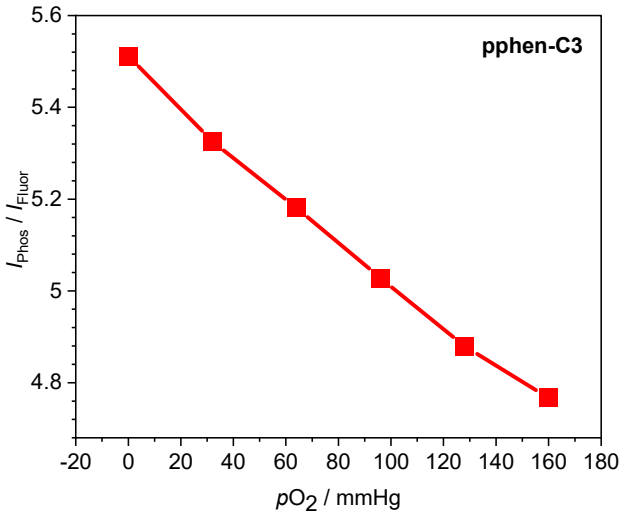

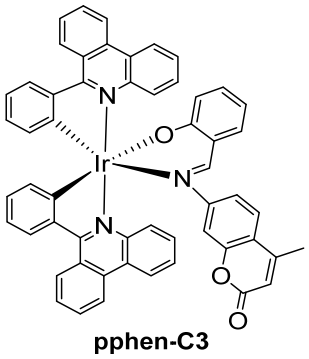

Fig. S33. Plot of the ratio of phosphorescence to fluorescence intensity of **pphen-C3**, recorded as a function of oxygen partial pressure (pO_2). The luminescence intensities were rerecorded as the maximum intensity values of the long-wavelength phosphorescence (I_{Phos}) and short-wavelength fluorescence (I_{Fluor}) bands.

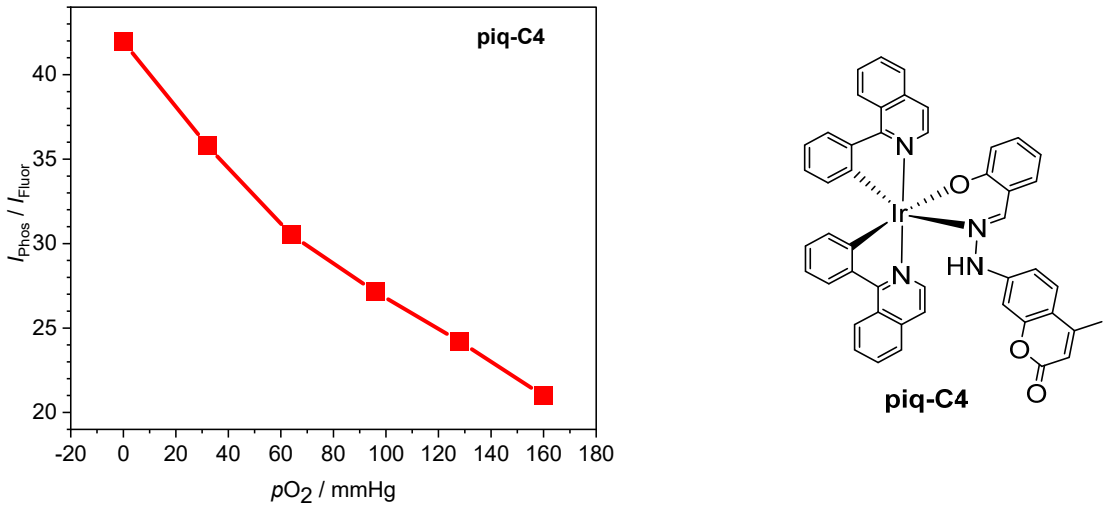

Fig. S34. Plot of the ratio of phosphorescence to fluorescence intensity of **piq-C4**, recorded as a function of oxygen partial pressure (pO_2). The luminescence intensities were rerecorded as the maximum intensity values of the long-wavelength phosphorescence (I_{Phos}) and short-wavelength fluorescence (I_{Fluor}) bands.

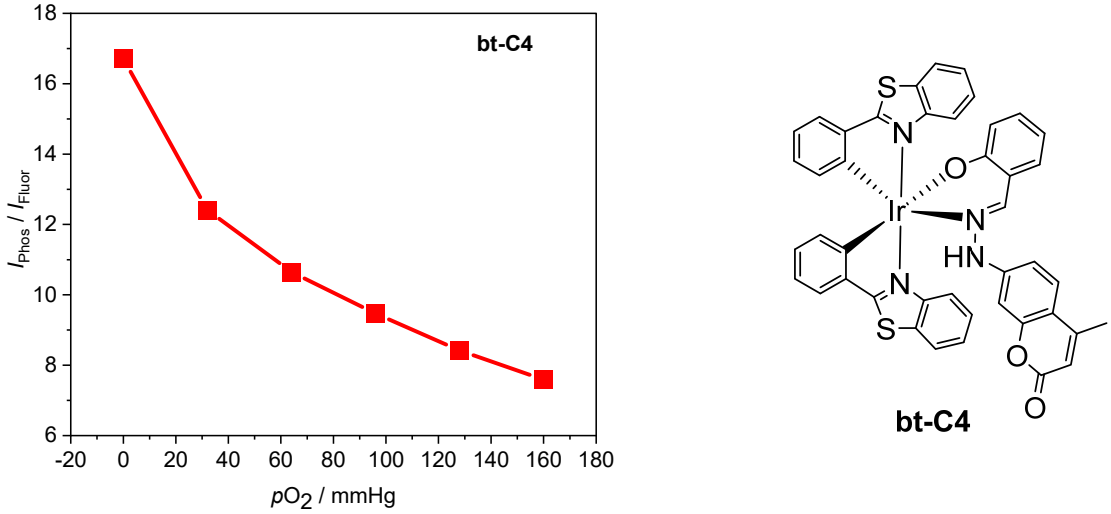

Fig. S35. Plot of the ratio of phosphorescence to fluorescence intensity of **bt-C4**, recorded as a function of oxygen partial pressure (pO_2). The luminescence intensities were rerecorded as the maximum intensity values of the long-wavelength phosphorescence (I_{Phos}) and short-wavelength fluorescence (I_{Fluor}) bands.

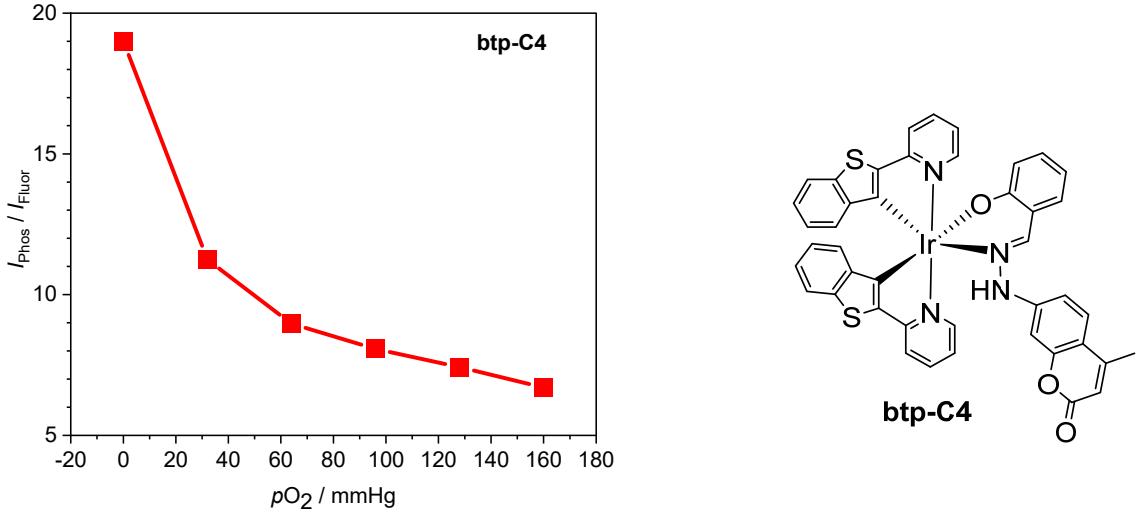

Fig. S36. Plot of the ratio of phosphorescence to fluorescence intensity of **btp-C4**, recorded as a function of oxygen partial pressure (pO_2). The luminescence intensities were rerecorded as the maximum intensity values of the long-wavelength phosphorescence (I_{Phos}) and short-wavelength fluorescence (I_{Fluor}) bands.

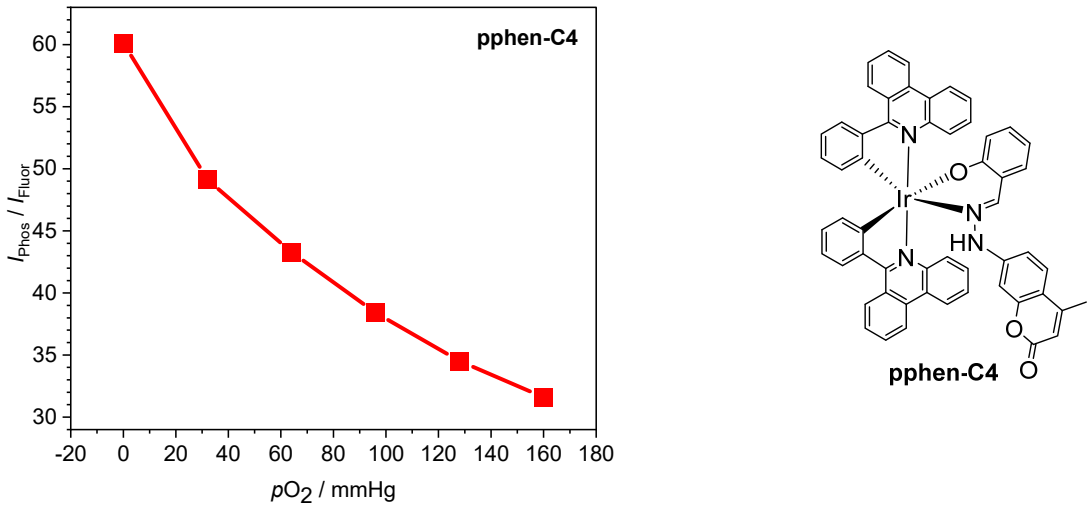

Fig. S37. Plot of the ratio of phosphorescence to fluorescence intensity of **pphen-C4**, recorded as a function of oxygen partial pressure (pO_2). The luminescence intensities were rerecorded as the maximum intensity values of the long-wavelength phosphorescence (I_{Phos}) and short-wavelength fluorescence (I_{Fluor}) bands.

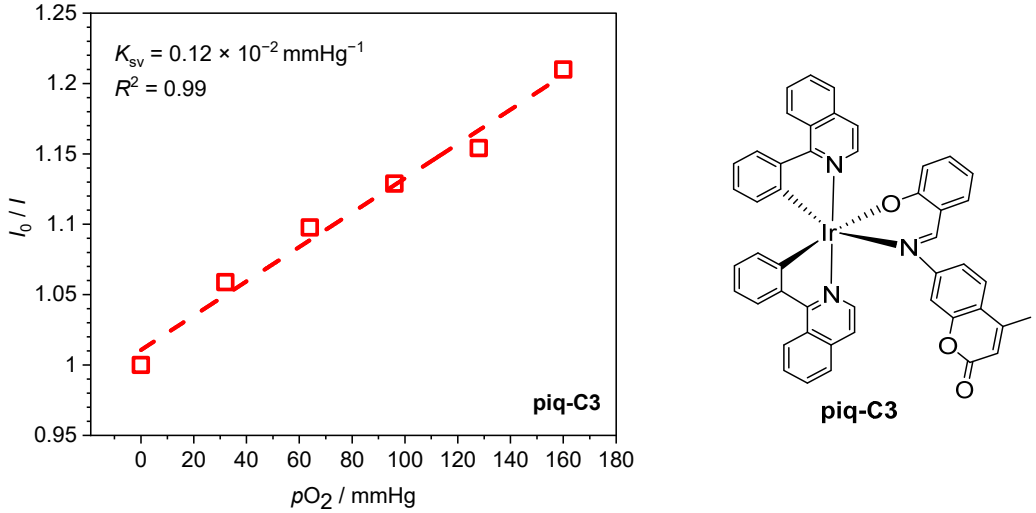

Fig. S38. Stern-Volmer plot of **piq-C3** fit using the phosphorescence intensity method stated in Equation 1 of the main text. The ratio I_0/I represents the ratio of phosphorescence intensity in the absence of oxygen to the phosphorescence intensity at a given partial pressure of oxygen. The Stern-Volmer constant K_{SV} is provided, along with the R^2 value of the best-fit line.

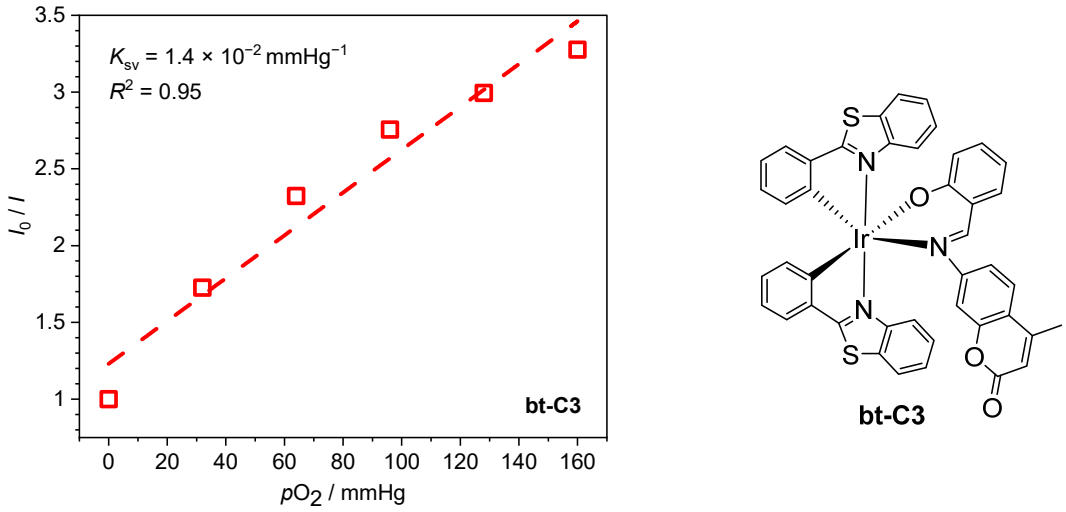

Fig. S39. Stern-Volmer plot of **bt-C3** fit using the ratiometric intensity method stated in Equation 1 of the main text. The ratio I_0/I represents the ratio of phosphorescence intensity in the absence of oxygen to the phosphorescence intensity at a given partial pressure of oxygen. The Stern-Volmer constant K_{SV} is provided, along with the R^2 value of the best-fit line.

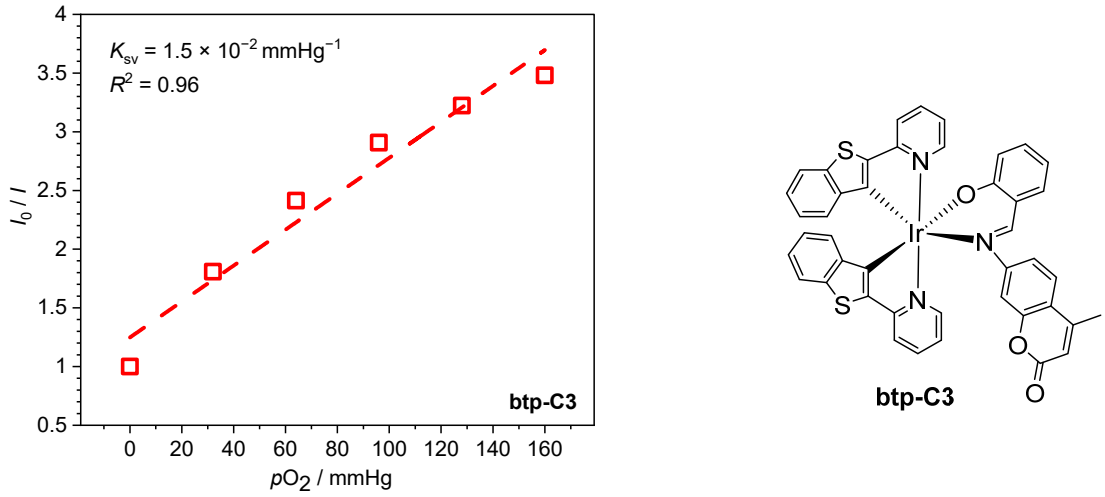

Fig. S40. Stern-Volmer plot of **btp-C3** fit using the ratiometric intensity method stated in Equation 1 of the main text. The ratio I_0/I represents the ratio of phosphorescence intensity in the absence of oxygen to the phosphorescence intensity at a given partial pressure of oxygen. The Stern-Volmer constant K_{SV} is provided, along with the R^2 value of the best-fit line.

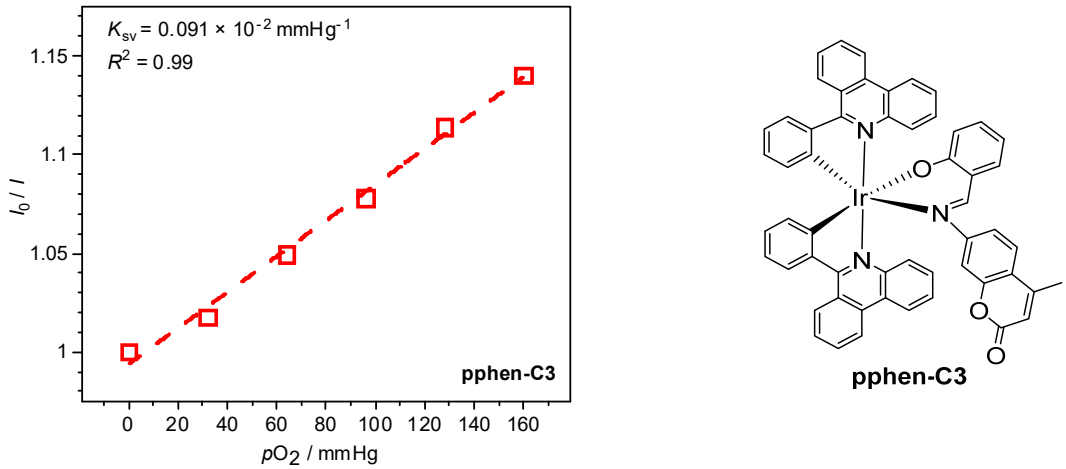

Fig. S41. Stern-Volmer plot of **pphen-C3** fit using the ratiometric intensity method stated in Equation 1 of the main text. The ratio I_0/I represents the ratio of phosphorescence intensity in the absence of oxygen to the phosphorescence intensity at a given partial pressure of oxygen. The Stern-Volmer constant K_{SV} is provided, along with the R^2 value of the best-fit line.

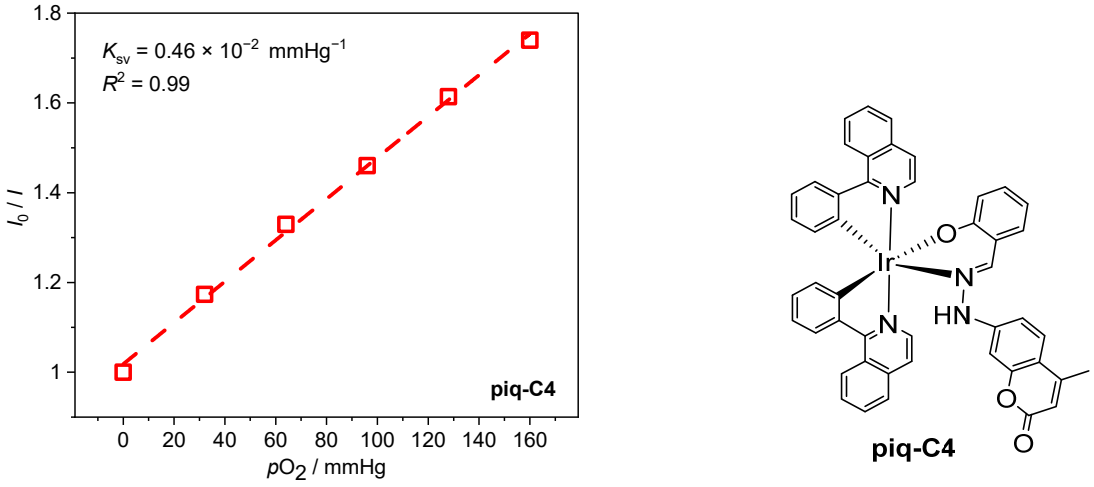

Fig. S42. Stern-Volmer plot of **piq-C4** fit using the ratiometric intensity method stated in Equation 1 of the main text. The ratio I_0/I represents the ratio of phosphorescence intensity in the absence of oxygen to the phosphorescence intensity at a given partial pressure of oxygen. The Stern-Volmer constant K_{SV} is provided, along with the R^2 value of the best-fit line.

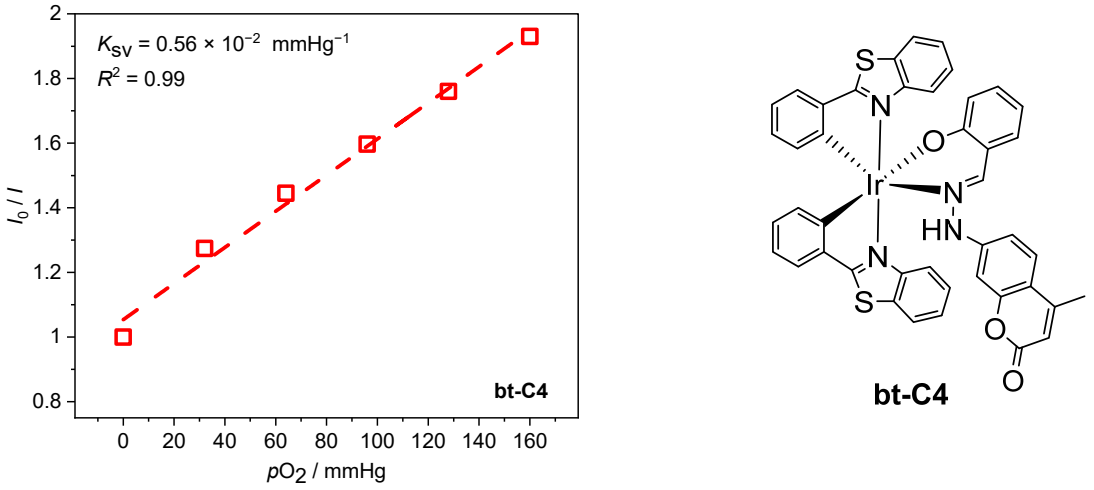

Fig. S43. Stern-Volmer plot of **bt-C4** fit using the ratiometric intensity method stated in Equation 1 of the main text. The ratio I_0/I represents the ratio of phosphorescence intensity in the absence of oxygen to the phosphorescence intensity at a given partial pressure of oxygen. The Stern-Volmer constant K_{SV} is provided, along with the R^2 value of the best-fit line.

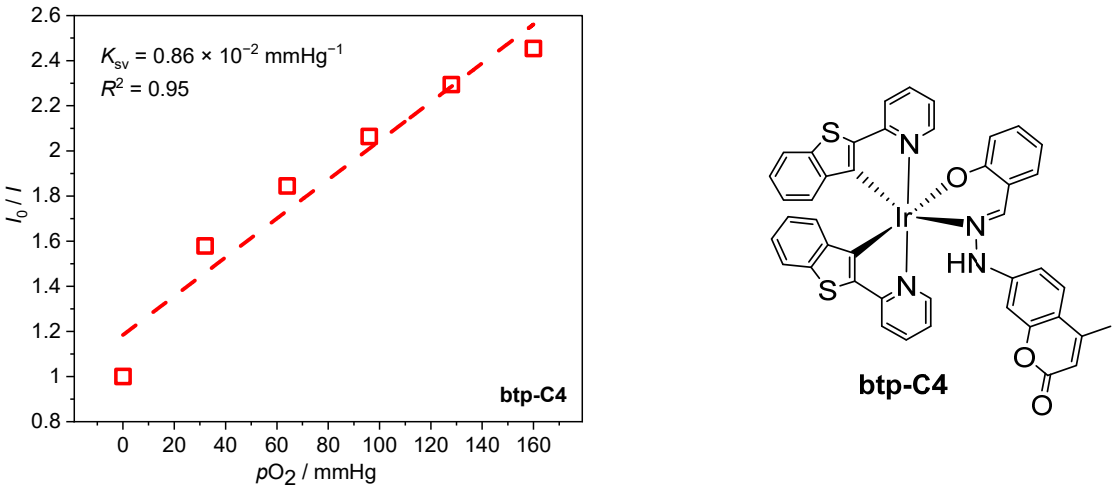

Fig. S44. Stern-Volmer plot of **btp-C4** fit using the ratiometric intensity method stated in Equation 1 of the main text. The ratio I_0/I represents the ratio of phosphorescence intensity in the absence of oxygen to the phosphorescence intensity at a given partial pressure of oxygen. The Stern-Volmer constant K_{SV} is provided, along with the R^2 value of the best-fit line.

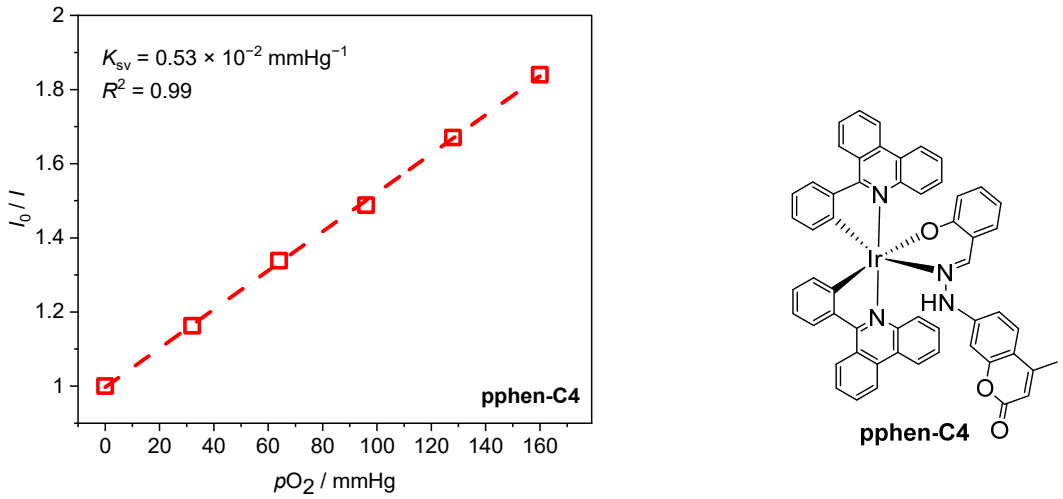

Fig. S45. Stern-Volmer plot of **pphen-C4** fit using the ratiometric intensity method stated in Equation 1 of the main text. The ratio I_0/I represents the ratio of phosphorescence intensity in the absence of oxygen to the phosphorescence intensity at a given partial pressure of oxygen. The Stern-Volmer constant K_{SV} is provided, along with the R^2 value of the best-fit line.

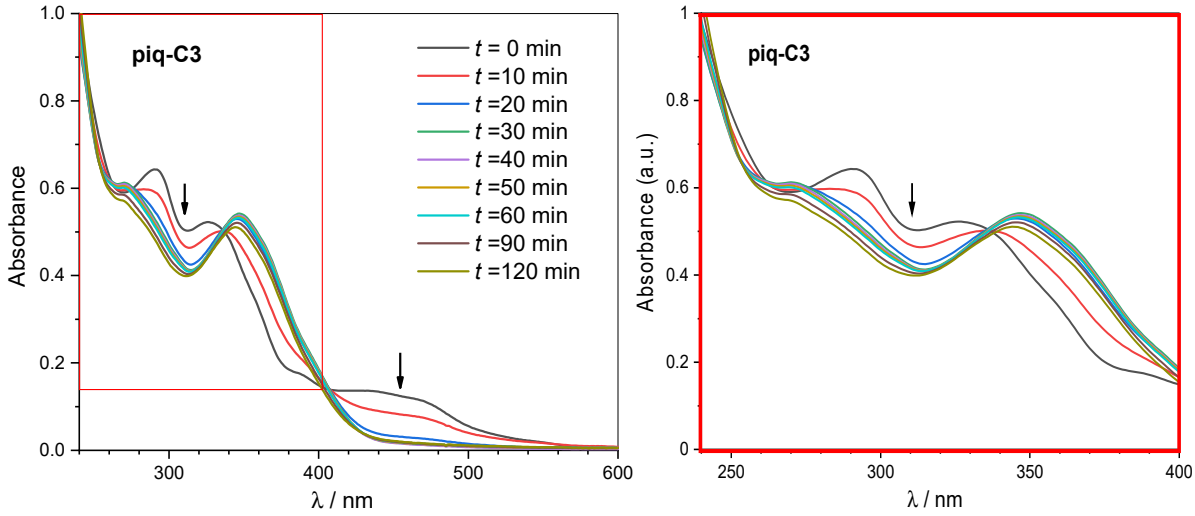

Fig. S46. Time evolution of the UV-vis absorption spectra of complex **piq-C3** upon irradiation with UV light, in CH_2Cl_2 under aerobic conditions.

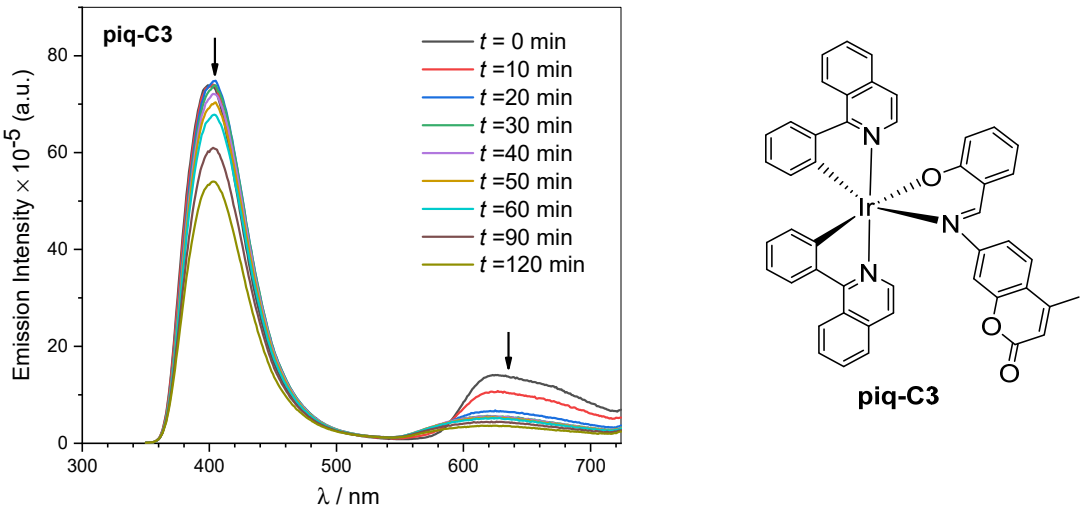

Fig. S47. Time evolution of the photoluminescence spectra of complex **piq-C3** upon irradiation with UV light, in CH_2Cl_2 under aerobic conditions.

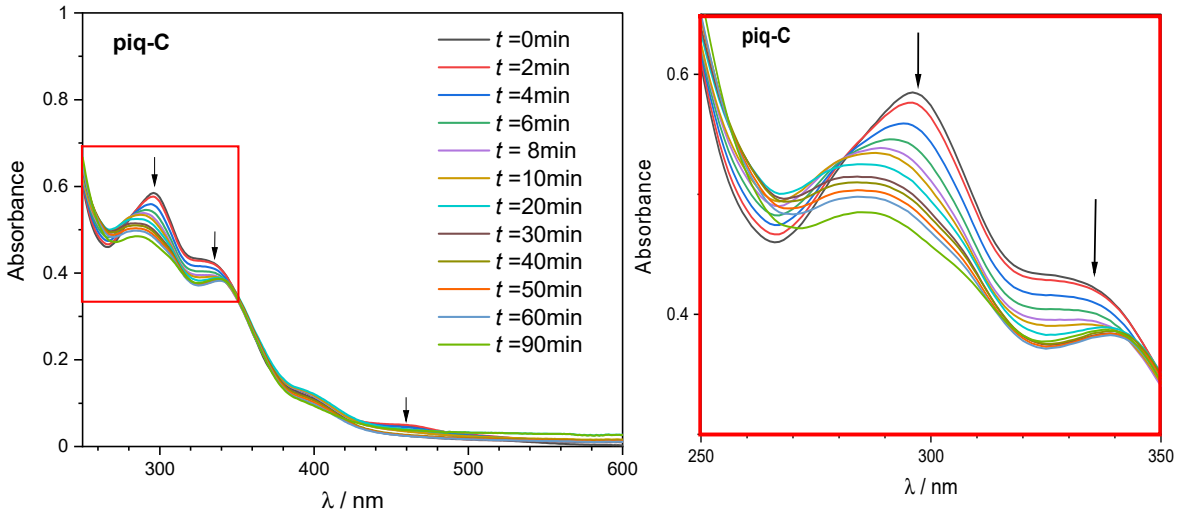

Fig. S48. Time evolution of the UV-vis absorption spectra of complex **piq-C** upon irradiation with UV light, in CH_2Cl_2 under aerobic conditions.

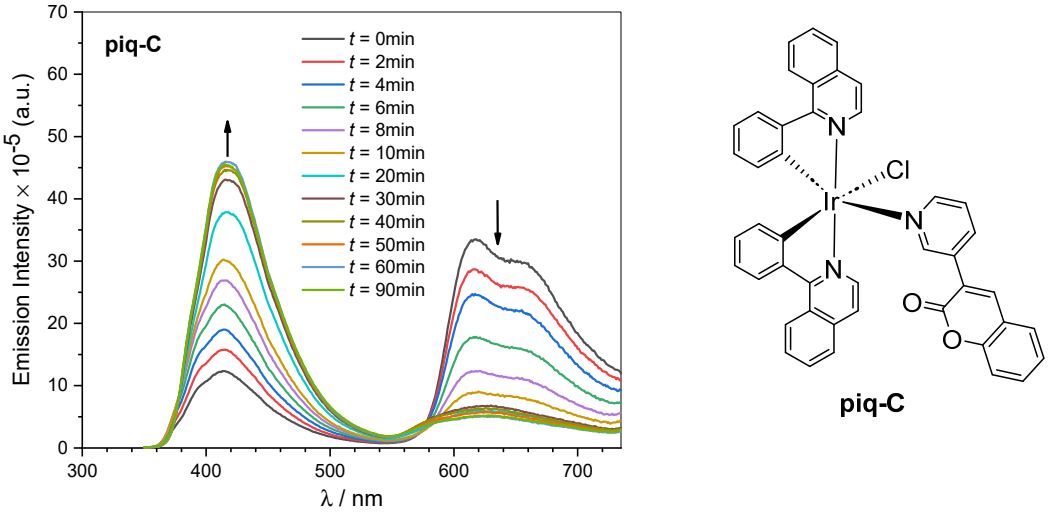

Fig. S49. Time evolution of the photoluminescence spectra of complex **piq-C** upon irradiation with UV light, in CH_2Cl_2 under aerobic conditions.

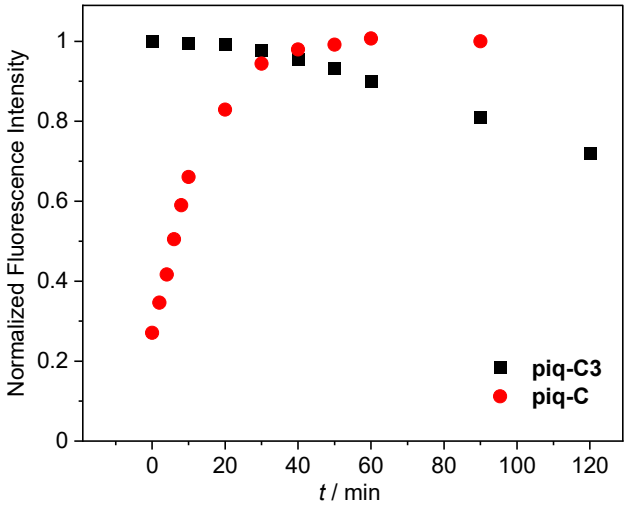

Fig. S50. Normalized fluorescence intensity as a function of time for **piq-C3** (black) and **piq-C** (red), observed at their respective fluorescence maxima.

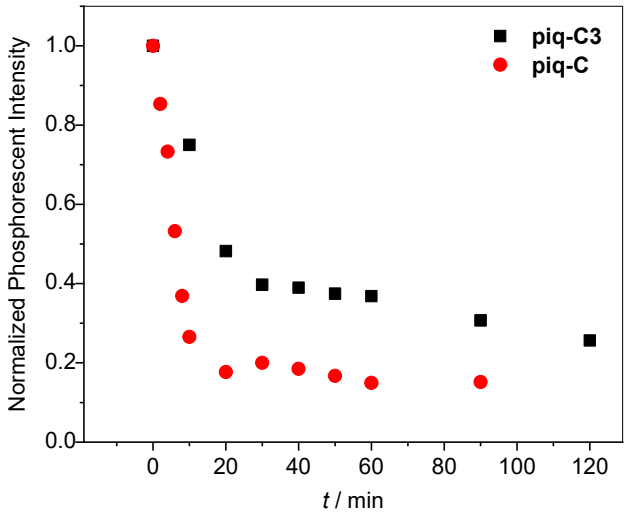

Fig. S51. Normalized phosphorescence intensity as a function of time for **piq-C3** (black) and **piq-C** (red), observed at their respective phosphorescence maxima.

Supporting Information References

1 M. Nonoyama, *Bull. Chem. Soc. Jpn.*, 1974, **47**, 767–768.
2 C. Liu, X. Liu, X. Ge, Q. Wang, L. Zhang, W. Shang, Y. Zhang, X. A. Yuan, L. Tian, Z. Liu and J. You, *Dalton Trans.*, 2020, **49**, 5988–5998.
3 A. Banerjee, T. D. Panosian, K. Mukherjee, R. Ravindra, S. Gal, D. L. Sackett and S. Bane, *ACS Chem. Biol.*, 2010, **5**, 777–785.
4 F. Vögtle, M. Plevoets, M. Nieger, G. C. Azzellini, A. Credi, L. De Cola, V. De Marchis, M. Venturi and V. Balzani, *J. Am. Chem. Soc.*, 1999, **121**, 6290–6298.
5 G. M. Sheldrick, *Acta Crystallogr. Sect. C Struct. Chem.*, 2015, **71**, 3–8.
6 G. D. Sutton, C. Jiang, G. Liu and T. S. Teets, *Dalton Trans.*, 2023, **52**, 3195–3202.